circOMA1 delivered by exosomes regulates DRD2-mediated prolactinoma resistance

QING RAO[1,2*], DIMIN ZHU[2*], ZONGMING WANG[2*], SHAOLIN ZHANG[2*], XUELI LI[1], SHASHIKIRAN TAGILAPALLI[2], NAN WANG[1], WEIYU HU[2], WENLI CHEN[2] and YONGHONG ZHU[1]

[1]Department of Histology and Embryology, School of Medicine, Sun Yat-sen University, Shenzhen, Guangdong 518107, P.R. China; [2]Department of Neurosurgery, The Sixth Affiliated Hospital, Sun Yat-sen University, Guangzhou, Guangdong 510060, P.R. China

Received October 11, 2025; Accepted March 9, 2026

DOI: 10.3892/ijmm.2026.5812

Abstract. Among pituitary adenomas, prolactin-secreting pituitary neuroendocrine tumours (PRL-PitNETs) are unique in that pharmacotherapy, specifically cabergoline (CAB), can be used as a first-line treatment, and it is the recommended therapeutic option. However, the mechanisms underlying CAB resistance remain incompletely understood. In the present study, gene microarray analysis and clinical tissue specimens were used to identify circular RNAs (circRNAs) associated with CAB resistance. circOMA1 expression was quantified in PRL-PitNET tissues and patient plasma using reverse transcription-quantitative PCR, and its diagnostic potential was evaluated in 219 patients with pituitary adenoma. Gain- and loss-of-function assays, combined with molecular biology techniques, were used to investigate the biological function of circOMA1 and the underlying molecular mechanism. circOMA1 was identified as a critical circular RNA influencing CAB resistance and prognosis in PRL-PitNET. Mechanistically, circOMA1 acted as a miR-145-5p sponge, leading to upregulation of the E3 ubiquitin ligase Kelch-repeat and BTB domain-containing protein 7. This promoted ubiquitination of the CAB-specific, high-affinity G-protein-coupled receptor dopamine D2 receptor. Consequently, downstream autophagy was attenuated, and AKT pathway inhibition was impaired, which underlied the resistance. Furthermore, *in vitro* and *in vivo* studies demonstrated that circOMA1 was transported via exosomes, facilitating the transmission of CAB resistance among PRL-PitNET cells. Plasma exosomal circOMA1 levels were significantly elevated in PRL-PitNET patients preoperatively. These findings established circOMA1 as a key mediator of CAB resistance and a potential prognostic indicator in patients with a PRL-PitNET.

Correspondence to: Professor Yonghong Zhu, Department of Histology and Embryology, School of Medicine, Sun Yat-sen University, 66 Gongchang Road, Guangming, Shenzhen, Guangdong 518107, P.R. China
E-mail: zhuyongh@mail.sysu.edu.cn

Professor Wenli Chen, Department of Neurosurgery, The Sixth Affiliated Hospital, Sun Yat-sen University, 26 Yuancun 2nd Cross Road, Yuancun, Tianhe, Guangzhou, Guangdong 510060, P.R. China
E-mail: chenwenli@mail.sysu.edu.cn

*Contributed equally

Key words: prolactinoma, hsa_circ_0002316, exosomes, drug resistance

Introduction

Pituitary adenomas (PAs), also known as pituitary neuroendocrine tumours (PitNETs), are among the three primary intracranial tumours, with an incidence of ~17.1% among intracranial neoplasms, while the prevalence of clinically symptomatic cases is estimated at ~1 in 1,100 individuals (1). Based on hormone hypersecretion status, PitNETs are classified as either a clinically non-functioning PitNET (NF-PitNET) or a hormone-secreting PitNET (2). According to the 2022 World Health Organization classification, which incorporates cell lineage, hormone composition, and specific histological and immunohistochemical (IHC) features, PitNETs are categorised into subtypes, including prolactin-secreting (PRL-PitNET), growth hormone-secreting (GH-PitNET), and adrenocorticotropic hormone-secreting (ACTH-PitNET) tumours, among others (3). PRL-PitNET is the most prevalent subtype, constituting ~53% of all PitNETs (1).

PRL-PitNET is currently the only PitNET type for which pharmacotherapy is the preferred management approach. Dopamine receptor agonists (DAs), including bromocriptine (BRC) and cabergoline (CAB), are first-line treatments for PRL-PitNET (4,5). Although most patients with a PRL-PitNET achieve excellent outcomes with DA therapy, 20-30% exhibit resistance to BRC, and 5-15% are resistant to CAB (6,7). Previous studies have identified decreased expression or activity of the dopamine D2 receptor (DRD2) as a primary cause of drug resistance in PRL-PitNET (8-11); however, the specific mechanisms underlying this remain incompletely understood. As PitNETs are predominantly benign tumours, reports of gene mutations are infrequent (12). Evidence suggests that dysregulation of epigenetic modifications may be a primary driver of PitNETs pathogenesis (13). Therefore, investigating alterations in post-transcriptional regulatory

mechanisms is clinically significant for the targeted therapy of PitNETs.

Non-coding RNAs (ncRNAs) can target and regulate signalling pathways, playing major roles in physiological and pathological processes. Circular RNAs (circRNAs) are a class of endogenous ncRNA characterised by a covalently closed loop structure, generated through back-splicing of precursor mRNA (14). This circular structure confers resistance to exonuclease degradation, resulting in greater stability compared with linear RNAs. Accumulating evidence indicates that circRNAs play critical roles in numerous tumour-related processes, including formation, drug resistance, progression and relapse. To date, the association between circRNAs, drug resistance in PRL-PitNET, and DRD2 expression/activity has not been elucidated.

Exosomes (30-150 nm in diameter) are nanoscale membrane vesicles derived from endosomal multivesicular bodies and released into the extracellular environment. Previous studies demonstrated that exosomal circRNAs exhibit high stability and tissue specificity, playing crucial roles in neoplasm processes such as drug resistance (15-17), diagnosis (18-20), treatment (21,22), prognosis (23,24), immunity (25), metabolism (26) and progression (27-29). For example, bone abnormalities associated with GH-PitNET may be partially mediated by exosomes carrying miR-21-5p, which targets PDCD4 to modulate the Smad7/Runx2 pathway (30). Additionally, Zhang *et al* (31) found that exosome-delivered lncRNA H19 reduced CAB resistance in GH3 cell lines, and plasma exosomal H19 served as a biomarker for predicting CAB response in patients with a PRL-PitNET. However, whether and how exosome-transmitted circRNAs induce CAB resistance in PRL-PitNET remains unknown. In our previous study using gene microarray assays (32) and experimental analysis, circOMA1 was shown to be associated with PRL-PitNET pathogenesis (33). In the present study, circOMA1 was shown to be upregulated in drug-resistant PRL-PitNET cells, and silencing circOMA1 substantially increased CAB sensitivity in PRL-PitNET cells. Mechanistically, circOMA1 functioned as a cytoplasmic miR-145-5p sponge, promoting Kelch-repeat and BTB domain-containing protein 7 (KBTBD7)-mediated DRD2 ubiquitination and consequently attenuating CAB-induced autophagy.

Materials and methods

Patient samples. Human prolactinoma specimens were obtained from patients undergoing an endoscopic endonasal transsphenoidal approach. Immediately after removal, the tumour tissue was placed in an ice box at 4˚C and transferred to the laboratory within 2 h for research or stored at -80˚C. In addition, whole blood was collected from 219 patients with PAs from the elbow vein. The present study was performed in accordance with the ARRIVE guidelines. All participants provided written informed consent, and the study was approved by the Ethics Committee of the First Affiliated Hospital of Sun Yat-sen University [approval no. (2020)090; Guangzhou, China]. DA resistance was defined as a lack of normalisation of prolactin (PRL) serum levels or associated volume reduction (maximum diameter reduction ≥30%) after treatment with standard DA doses (7.5-10 mg BRC daily or 2.0 mg CAB weekly) for at least 6 months. The patient's postoperative blood samples were collected at 1-7 days after surgery. Tissues from 6 cases of drug-sensitive PitNET (PRL-PitNET-S) and 14 cases of drug-resistant PitNET (PRL-PitNET-R) were collected. The clinical-pathological information is shown in Tables SI and SII.

Cell culture, plasmids and reagents. MMQ rat prolactinoma cells were obtained from ATCC (cat. no. CRL-10609) and cultured in DMEM/F12 (Gibco; Thermo Fisher Scientific, Inc.) supplemented with 10% FBS (Shanghai ExCell Biology, Inc.), 100 U/ml penicillin, and 100 μg/ml streptomycin (Nanjing KeyGen Biotech Co., Ltd.). 293T cells were obtained from ATCC (cat. no. CRL-11268) and cultured in DMEM supplemented with 10% FBS, 100 U/ml penicillin, and 100 mg/ml streptomycin. Cells were maintained in a humidified incubator supplied with 5% CO_2 at 37˚C or stored in liquid nitrogen in serum-free cell freezing medium (cat. no. CS0401; GenKern Biotechnology).

Exosome isolation. MMQ cells stably overexpressing exogenous circOMA1 using a lentiviral vector were established (termed circOM), with cells transduced with an empty lentiviral vector serving as the control (termed circNC). The circular structure of circOMA1 was identified by amplification with junction-spanning primers and Sanger sequencing. The exosomes in the supernatant from circOM or circNC cells were extracted by differential ultracentrifugation. Briefly, the cells were cultured in complete DMEM/F12, and when required, the media replaced with serum-free DMEM/F12 medium for 24 or 48 h. The supernatant was collected and centrifuged through 2,000 x g for 20 min at 4˚C, followed by 10,000 x g for 30 min. After discarding the sediments, the supernatant was filtered through 0.22-μm filters (MilliporeSigma), followed by ultracentrifugation at 110,000 x g for 70 min through a Type 70Ti rotor at 4˚C (Beckman Coulter, Inc.). Subsequently, the pellets were resuspended in PBS and purified by ultracentrifugation at 110,000 x g for 70 min at 4˚C. Subsequently, the exosomes were resuspended in PBS for co-culture or experimental use, or stored at -80˚C. All centrifugation conditions were at 4˚C.

Extraction of genomic DNA (gDNA) and DNA electrophoresis. gDNA Extraction from circOM cells was performed using the SteadyPure Universal Genomic DNA Extraction Kit (cat. no. AG21009; Accurate Biology) according to the manufacturer's protocol. The product was then amplified by qPCR and visualised on a 2% agarose gel using Safe Green (Biosharp Life Sciences). The DNA polymerase used was included in SYBR Green Premix Pro Taq HS qPCR Kit (cat. no. AG11701; Accurate Biology). The sequences of forward and reverse primers were as follows: CircOMA1 forward, 5'ACCCAAGAT GCCAGAATGGT-3' and reverse, 5'-TTGATGACAGCCCCG TGAG-3'; OMA1 forward, 5'-CGGTTCCTCTCTTGTTGA-3' and reverse, 5'-GTAGCTTGCTCCTTCCTG-3'; GAPDH forward, 5'-GCGAGATCCCTCCAAAAT-3' and reverse, 5'-GTCCTTCCACGATACCAA-3'. The thermocycling conditions were as follows: Preheat at 95˚C for 30 sec, followed by 40 cycles of 95˚C for 5 sec and 60˚C for 30 sec.

Actinomycin D and RNase R assay. circOM cells were treated with 0.5 μg/ml actinomycin D (cat. no. HY-17559; MedChemExpress), and RNA was extracted at different time points (0, 6, 12, 18 and 24 h). Reverse transcription-quantitative (RT-qPCR) was used to detect the stability of RNA. For RNase R assays, equal quantities of total RNA (1 μg) with or without 3 U/μg RNase R (Guangzhou Geneseed Biotech. Co., Ltd.) were incubated at 37˚C for 15 min and 70˚C for 10 min. Subsequently, RT-qPCR was used to detect the abundance of target genes, and the products were visualised by DNA electrophoresis on a 2% agarose gel.

RNA isolation and RT-qPCR. Total RNA was extracted from MMQ and 293T cells, clinical samples, and exosomes using TRIzol® reagent (Invitrogen; Thermo Fisher Scientific, Inc.) according to the manufacturer's instructions. Nuclear and cytoplasmic RNA was extracted using a Nuclear/cytoplasmic separation kit (cat. no. BB-36021; Bestbio; https://www.beibokit.com/). Reverse transcription of total RNA into cDNA was performed using PrimeScript™ RT MasterMix (Takara Bio, Inc.) or a miRNA first-strand cDNA synthesis kit (Accurate Biology) according to the manufacturer's instructions. qPCR was performed using Genious 2X SYBR Green Fast qPCR MIX (ABclonal Biotech Co., Ltd.). The thermocycling conditions were as follows: Preheat at 95˚C for 30 sec, followed by 40 cycles of 95˚C for 5 sec and 60˚C for 30 sec. To quantify circRNA, mRNA, and miRNA expression levels, the $2^{-\Delta\Delta Cq}$ method was used (34), with GAPDH or U6 as the internal control to normalise target gene expression. U6 and GAPDH were used as nuclear and cytoplasmic controls, respectively. The experiment was performed at least three times. Primer sequences are listed in Table SIII.

Western blot analysis. Total protein was extracted from circOM, 293T cells, PRL-PitNETs tissues, and exosomes using RIPA lysis buffer (Jiangsu CoWin Biotech Co., Ltd.), quantified using BCA (Jiangsu CoWin Biotech Co., Ltd.), and then 20-50 μg of protein was loaded on 8, 10, or 12% SDS-gels by SDS-PAGE, and subsequently transferred to a 0.22-μm or 0.45-μm PVDF membrane (MilliporeSigma). Subsequently, membranes were blocked with 5% skimmed milk for 1 h and incubated overnight with the primary antibody at 4˚C. Finally, the membranes were incubated in horseradish peroxidase (HRP)-conjugated goat anti-rabbit IgG (H+L) or HRP-conjugated goat anti-mouse IgG (H+L) secondary antibody at room temperature for 2 h. Signals were visualised using an ImageQuant Las4000mini with enhanced chemiluminescence reagent (MilliporeSigma). Information on the antibodies used is listed in Table SIV. ImageJ v1.8.0 (National Institutes of Health) was used for densitometric analysis.

5-EdU assay. The sterile coverslips were coated with 100 μg/ml polylysine (Beyotime Institute of Biotechnology) in 24-well plates, and $1x10^5$ cells were added for overnight culture. Then, 10 μM EdU solution (Beyotime Institute of Biotechnology) was added to the cells and incubated for 2 h at room temperature. Subsequently, the cells were fixed with 4% paraformaldehyde for 20 min at room temperature, washed, and permeabilised with 0.3% Triton X-100. Next, a click-reaction was performed according to the protocols (cat. no. C0075S; Beyotime Institute of Biotechnology). Hoechst 33342 was used to stain the nucleus for 10 min at room temperature. Images were observed using confocal laser microscopy.

Immunoblotting and co-immunoprecipitation (Co-IP). For the Co-IP assay, cells were lysed using 500 μl IP lysis buffer with PMSF (cat. no. abs955; Absin) after washing with pre-cooled PBS. The lysate was centrifuged at 14,000 x g for 10 min at 4˚C and incubated with the indicated primary antibody or rabbit anti-IgG antibody as a negative control. Then, the compound was gently rotated overnight at 4˚C. After incubation, 5 μl Protein A and 5 μl Protein G were added, and the mixture was gently mixed at 4˚C for 3 h. The centrifuged particles were washed 4 times with a washing buffer, 1X SDS buffer was added, and the sample was boiled at 100˚C for 5 min for western blotting.

Cycloheximide (CHX) assay. CHX (a protein synthesis inhibitor) and MG132 (a proteasome inhibitor) were purchased from MedChemExpress. circOM, circNC or MMQ cells were treated with 100 μg/ml CHX alone or combined with 20 μM MG132 for 0, 4, 8, or 12 h, after which, western blotting was performed.

RFP-GFP-LC3 assay. circNC or circOM cells were seeded into sterile 6-well plates and incubated for 1 day. RFP-GFP-LC3 plasmids were transfected into cells using Liposome® 3000 (Thermo Fisher Scientific, Inc.) using 3 μg of RFP-GFP-LC3 plasmid at room temperature. After 48 h, the media was replaced, and the cells were treated with CAB. The following day, cells were fixed with 4% paraformaldehyde for 20 min and nuclei were stained using 1 μg/ml DAPI for 10 min at room temperature. Subsequently, cells were imaged using a confocal microscope.

Lentivirus and stable cell line construction. The sgRNA primer sequences of KBTBD7 were designed by CHOPCHOP (chopchop.cbu.uib.no/). sgRNA1 is designed to target positions 2067-2086bp of the target gene, while sgRNA2 targets positions 570-589 bp. The sgRNA sequences (sgRNA1 forward, 5'-CACCGAGTATATGAATACGACACTA-3' and reverse, 5'-AAACTAGTGTCGTATTCATATACTC-3'; and sgRNA2 forward, 5'-CACCGCTTCAAGAGCATG TTCACAG-3' and reverse, 5'-AAACCTGTGAACATG CTCTTGAAGC-3') were synthesised by Beijing Qingke Biotechnology Co., Ltd. Phosphorylate and oligos (sgRNAs) were inserted into a LentiCRISPRv2 vector (cat. no. 52961; Addgene, Inc.), linearised by restriction endonuclease using *BsmBI* (cat. no. R0739; New England BioLabs, Inc.) using T4 ligase. 293T cells were plated in a 10-cm culture dish and cultured until 80% confluent. The constructed target plasmid LentiCRISPRv2 and packaging plasmids psPAX2 (cat. no. 12260; Addgene, Inc.) and pMD2.G (cat. no. 12259; Addgene, Inc.) were transfected using Liposome® 3000 with a ratio of 5 μg: 5 μg: 5 μg. After 48 h of transfection, the supernatant containing lentiviral particles (generation system used, 2nd; MOI used to infect cells, 20) from 293T cells was collected and filtered through a 0.45-μm filter (MilliporeSigma) for subsequent MMQ cell infection. After 6 h of infection with lentiviral particles, the media from the MMQ cells was

replaced with fresh media. After 48 h, the level of endogenous protein was then verified by western blotting, and puromycin (2 μg/ml) was added to select for successfully transfected cells for 1 week. Finally, a stable gene-knockdown MMQ cell line was obtained via the limited dilution method.

Cell viability and colony formation assays. For the cell activity assay, $3x10^3$ cells were plated in 96-well plates and incubated at specified time points with or without CAB (cat. no. HY-15296; MedChemExpress). The minimum number of cells considered to form a colony was 50. Subsequently, Cell Counting Kit-8 (CCK-8) solution (Dojindo Molecular Technologies, Inc.) was added (10 μl/well), and the mixture was incubated at room temperature for 2 h. Absorbance was measured using a microplate reader (Tecan Group, Ltd.) at 450 nm. The cells were seeded into 24-well plates (100 cells/well) coated with 100 μg/ml polylysine (Beyotime Institute of Biotechnology). After culturing for 2 weeks, the cells were fixed with 4% paraformaldehyde (Biosharp Life Sciences) for 20 min and stained with 1% crystal violet (MilliporeSigma) for 15 min at room temperature. Images of the colonies were captured using a Fluorescent (enzyme-linked) spot analyser (S6 ULTRA; Cellular Technology Limited).

Luciferase reporter assay. A total of $1x10^4$ MMQ cells/well were plated in 96 wells. When confluence reached 70-80%, miR-145-5p mimics or miR-NC (50 nmol/l) and fluorescent reporter plasmid (50 ng/well, pmirGLO constructs with WT or mutated target sequence) were co-transfected using Lipofectamine® 3000 (Invitrogen; Thermo Fisher Scientific, Inc.). After 24 h of transfection, firefly luciferase activity was normalised to *Renilla* luciferase activity using the luciferase reporter assay system (Promega Corporation).

Immunofluorescence assays. Cells were washed three times with PBS, then cells or tissues were fixed with 4% paraformaldehyde for 20 min at room temperature and permeabilised with 0.2% Triton X-100 for 10 min at room temperature. Subsequently, after blocking with 10% goat serum (MilliporeSigma) at room temperature for 1 h, the cells or tissues were incubated with corresponding primary antibodies overnight at 4˚C. Next, cells or tissues were incubated with a fluorescent secondary antibody at room temperature for 1 h, followed by staining with 1 μg/ml DAPI for 5 min. Each step required three 15 min washes with PBS. Fluorescence images were obtained using a confocal laser scanning microscope.

RNA-FISH. The circOMA1 hybridisation probe was designed and synthesised by Shanghai GenePharma, Co., Ltd. RNA-FISH was performed on circOM cells and tissues using an *in-situ* hybridisation kit (Exon Biotech Inc.), according to the manufacturer's protocol. Images were obtained on a Nikon C2 laser-scanning confocal microscope. The FISH probe was labelled with digoxigenin, and the sequence was 5'-CACTTGACTACCTGAGGTATAAG-3'.

Vector construction and cell transduction. circOMA1 small interfering (si)RNA (5'-ACCUCAGGUAGU CAAGUGATT-3'), miR-145-5p mimic (5'-GUCCAG UUUCCCAGGAAUCCCU-3'), miR-145-5p inhibitor (5'-AGGGAUUCCUGGGAAAACUGGAC-3'), and the corresponding negative controls were designed and synthesised by Beijing Qingke Biotechnology Co., Ltd. A total of $4x10^4$ cells/well (circOM or circNC) were plated in a 24-well plate, when the cell density was ~80%, and DMEM/F12 medium without penicillin/streptomycin was added. The miR-145-5p mimic (30 nM) and miR-145-5p inhibitor (50 nM) were transfected using Lipofectamine® 3000 (cat. no. L3000-015, Thermo Fisher Scientific, Inc.), and the control group was set up by transfecting the control vector. After 24 h of transfection at room temperature, subsequent experiments were performed immediately.

Ubiquitination assay. CircOM or circNC cells were lysed in RIPA lysis buffer and centrifuged at 10,000 x g for 10 min at 4˚C. Supernatants containing 500 μg total protein were transferred to fresh 1.5-ml tubes and incubated with the appropriate anti-DRD2 primary antibody or control IgG with gentle rotation for 2 h at 4˚C. A total of 20 μl of Protein A/G magnetic beads was added, and the mixtures were rotated overnight at 4˚C. Immunocomplexes were collected by centrifugation at 1,000 x g for 5 min at 4˚C, washed four times with cold RIPA buffer, resuspended in 40 μl 1X SDS sample buffer, and boiled for 5 min. Ubiquitin conjugation of DRD2 was detected by western blotting.

Haematoxylin-eosin and IHC staining. The xenograft tumours were removed, fixed with 4% paraformaldehyde at room temperature, paraffin-embedded and then sectioned (4-μm thick). Sections were dewaxed with xylene and hydrated (by sequential immersion in 100, 95, 85, and 70% ethanol for 5 min per solution), then stained with H&E or antigen retrieval (citrate buffer solution) at room temperature. After the endogenous peroxidase was blocked with 3% hydrogen peroxide for 10 min, and blocked using 10% goat serum for 30 min at room temperature, samples were incubated with primary antibody overnight at 4˚C. Finally, the sections were incubated with DAB (Jiangsu CoWin Biotech Co., Ltd.) and observed under a fluorescence microscope (DMI4000B; Leica Microsystems GmbH).

Co-culture assay. circOM or circNC cells were co-cultured with the parental cells using a 0.4-μm Transwell chamber (Corning, Inc.) for 5-7 days. After co-culture, the sensitivity of parental cells to CAB was measured using a CCK-8 assay. Separately, 30 μg/ml exosomes from the supernatant of circOM or circNC cells were co-cultured with parental cells for 24, 48, or 72 h. Subsequently, parental cells were collected for subsequent experimental studies.

Exosome labelling. Exosomes from circOM or circNC cell supernatants were labelled using a diluted PKH67 (a fluorescent dye, Beijing Fluorescence Biotechnology Co., Ltd.) to ensure a final concentration of 4 μM. Cells were incubated for 5 min and gently mixed. Subsequently, 10% FBS without exosomes containing an excess of dye was diluted with PBS and centrifuged at 4˚C, 110,000 x g for 70 min to remove any unbound dye. The supernatant was discarded, and the exosomes were washed twice in PBS by centrifugation at 110,000 x g.

Nanoparticle tracking analysis (NTA). NTA of exosomes derived from circOM or circNC cell supernatant was performed using a Flow Nanoanalyzer (NanoFCM, U30) to measure the concentration, size, and distribution of exosomes.

Transmission electron microscopy (TEM). circOM or circNC cells were treated with 2.5% glutaraldehyde at 4˚C. After washing with PBS three times (5 min per wash), cells were fixed using 1% osmium tetroxide for 2 h at 4˚C and washed as aforementioned. Samples were dehydrated with a gradient of ethanol solutions (50, 70, 80, 90, and 100% for 10 min each), followed by 100% ethanol for another 10 min. Samples were dehydrated twice in acetone for 10 min each, then infiltrated with acetone and embedding solution at 3:1 for 30 min and 1:1 for 4 h, followed by overnight incubation in pure embedding solution at 4˚C. After embedding, polymerisation was performed at 37˚C for 24 h, followed by 60˚C for 48 h. Ultrathin sections of 50-70 nm were obtained and double-stained with 3% uranyl acetate for 30 min and lead citrate for 15 min at room temperature. For the exosome assay, samples were purified from cellular supernatant or plasma via differential ultracentrifugation, and 20 μl of the suspension was placed on a clean slide. A copper grid was floated on the droplet for 2 min to allow for sample adsorption, after which excess liquid was removed using filter paper to leave a thin film. The grid was then floated on a droplet of 1% phospho-tungstic acid for 2 min, wicked with filter paper, and dried passively at room temperature. All samples were observed and imaged using a TEM (Tecnai G2 Spirit Twin) at an accelerating voltage of 100 kV.

Xenograft mouse model. A total of 20 female old BALB/c nude mice (4-6 weeks old; weighing 14-16 g) were purchased from the East Campus of Sun Yat-sen University and raised in specific pathogen-free conditions, with a 12/12-h light/dark cycle, with the temperature maintained at 26˚C and humidity maintained at 50%. All the animal experiments were approved by the Animal Ethics Committee of Sun Yat-sen University (approval no. SYSU-IACUC-MED-2024-B014). circOMA1 was transfected into MMQ cells using a lentiviral vector (circOM) or a blank vector (circNC). A total of $1x10^6$ MMQ cells, circOM, or circNC cells were mixed in DMEM/F12 medium and high concentration Matrigel at a ratio of 1:1 (Shanghai Yeasen Biotechnology Co., Ltd.) and were respectively injected subcutaneously into the right flank or left flank of female BALB/c nude mice (the total injection volume was 100 μl, containing $1x10^6$). The volume of xenograft tumours was recorded every 3 days using calliper measurements of length and width, and the formula volume=length x width/2. After 15 days, the mice were euthanised using 150 mg/kg sodium pentobarbital, the tumours were excised, and the weights of the neoplasms were measured immediately. Based on age and weight, BALB/c nude mice were matched and assigned to groups with corresponding identification numbers. Tumour volume and weight were measured in BALB/c nude mice by investigators blinded to group assignment and numbering. If a tumour in a BALB/c nude mouse exhibited extensive ulceration or reached a maximum diameter of >15 mm, the mouse was euthanised ahead of schedule. For exosome transmission resistance assays, $3x10^6$ MMQ cells were mixed with DMEM/F12 medium and a high-concentration matrix at a 1:1 ratio, inoculated subcutaneously into nude mice, and randomly divided into two groups after tumour formation; the total injection volume was 100 μl. The number of nude mice in each group was 5. On day 10, 1,1'-Dioctadecyl-3,3,3',3'-tetramethylindodicarbocyanine perchlorate (cat. no. KGMP0025; Nanjing KeyGen Biotech Co., Ltd.) labelled exosomes derived from circOM or circNC (100 μg/mouse, tail vein injection) combined with CAB (0.5 mg/Kg, intraperitoneal injection) were administered. To reduce discomfort, a human insulin syringe with a thinner needle was used. After 24 h, the distribution of exosomes in the subcutaneous tumour, brain, and pituitary gland of nude mice was observed using a microscopic living imaging system (cat. no. IVM-MS2; IVM Technology). Additionally, macroscopic live-imaging technology was used to observe exosome distribution in the hearts, livers, spleens, lungs and kidneys of nude mice (IVIS Spectrum). Exosomes and CAB were injected twice a week for 2 weeks. Intravenous tail vein injections of exosomes and CAB administration were performed by personnel who were not involved in the tumour modelling procedure. If a BALB/c nude mouse exhibited extensive ulceration or a tumour reached a diameter of >15 mm, the mouse was euthanised ahead of schedule. At the end of the procedure, mice were euthanised and tumours excised for subsequent analysis.

Bioinformatics prediction and database analysis. The regulatory axis between miR-145-5p and the target gene KBTBD7 was analyzed through TargetScan (https://www.targetscan.org/vert_72/), miRWalk (http://mirwalk.umm.uni-heidelberg.de/) and miRDB (https://mirdb.org/index.html). The expression levels of plasma exosomal circOMA1 in healthy individuals, benign conditions, and patients with different types of tumors were analyzed using the exoRBase V2 database (http://www.exorbase.org/exoRBaseV2/help/toIndex).

Statistical analysis. GraphPad Prism (version 8.0, GraphPad Software, Inc.; Dotmatics) was used for statistical analyses. Student's t-test (parametric data) or a paired t-test (non-parametric data) was used to analyse the differences in statistics between both groups. IC_{50} calculations were performed, and bar charts and line plots were generated using GraphPad. Data are presented as the mean ± SEM. $P<0.05$ was considered to indicate a statistically significant difference.

Results

CircOMA1 expression is upregulated in drug-resistant PRL-PitNET. The authors' previous gene microarray assay (32) and bioinformatics analysis identified circOMA1 as closely associated with PitNETs occurrence and development (33). To investigate its potential role in PRL-PitNET resistance and progression, circOMA1 expression was assessed in drug-sensitive prolactinoma (PRL-PitNET-S) and drug-resistant prolactinoma (PRL-PitNET-R) tissues, which revealed significantly higher circOMA1 expression in PRL-PitNET-R tissues (Fig. 1A). Due to the scarcity of human-derived PitNET cell lines, MMQ rat prolactinoma cells were used. MMQ cells stably overexpressing exogenous circOMA1 using a lentiviral vector were established (termed circOM), with

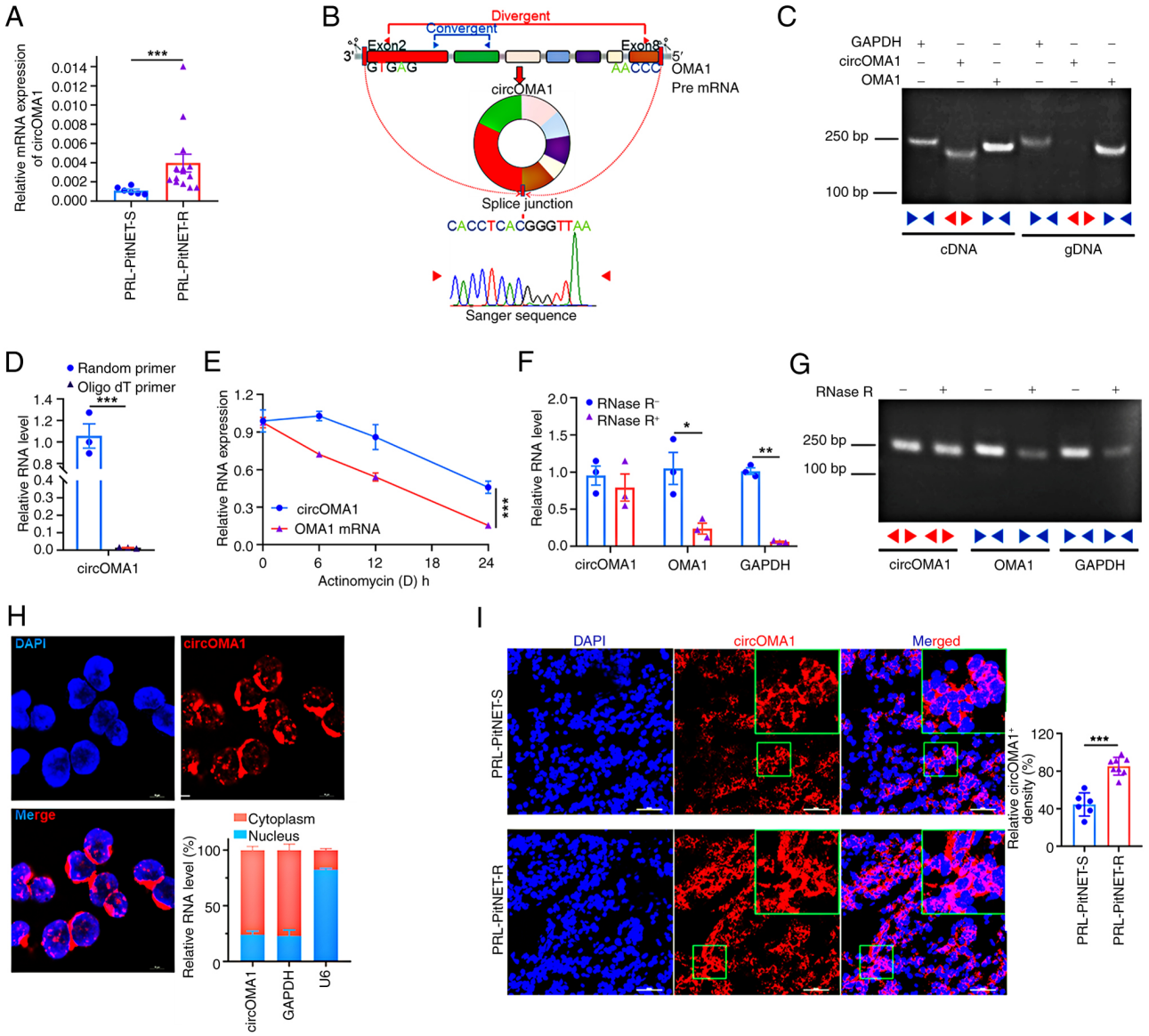

Figure 1. Characteristics and distribution of circOMA1 in PRL-PitNETs. (A) circOMA1 expression in PRL-PitNET-S (n=6) and PRL-PitNET-R (n=14) tissues. (B) Illustration of the annotated genomic region of circOMA1 verified by Sanger sequencing. (C) Amplification of the linear or back-splicing products was performed using cDNA and gDNA extracted from circOM-transfected cells using random primers and detected using agarose gel electrophoresis. (D) The random primer or Oligo dT primers used to amplify circOMA1. (E) Linear and circOMA1 expression levels were measured in circOM cells treated with actinomycin D at different time points using RT-qPCR. (F and G) RT-qPCR or agarose gel electrophoresis was used to detect the linear or circOMA1 expression levels of total RNA from circOM cells with or without RNase R treatment. (H) RNA-FISH and nuclear cytoplasmic separation were used to detect the distribution and expression of circOMA1 in circOM cells. Scale bar, 10 μm. (I) Representative image of the distribution and expression of circOMA1 in PRL-PitNET-S (n=6) and PRL-PitNET-R (n=8) tissues. Scale bar, 50 μm. Data are presented as the mean ± SEM. n≥3. Differences between groups were compared using a unpaired Student's t-test. *P<0.05, **P<0.01 and ***P<0.001. circ, circular RNA; PRL-PitNET, prolactin-secreting pituitary neuroendocrine tumour; PRL-PitNET-S, drug-sensitive PRL-PitNET; PRL-PitNET-R, drug-resistant PRL-PitNET; gDNA, genomic DNA; RT-qPCR, reverse transcription-quantitative PCR.

cells transduced with an empty lentiviral vector serving as the control (termed circNC).

circOMA1 (hsa_circ_0002316) is a 1,381bp transcript generated by back-splicing of exons 2-8 of the OMA1 gene. Its head-to-tail splice junction was confirmed by RT-qPCR and Sanger sequencing (Fig. 1B). Specific amplification of the splice junction occurred only with cDNA templates derived from circOM cells, not with genomic DNA (gDNA) templates (Fig. 1C). Furthermore, circOMA1 was amplified using random primers but not oligo(dT) primers, confirming it lacked a polyadenylated tail (Fig. 1D). To assess stability, circOM cells were treated with actinomycin D (an RNA synthesis inhibitor). circOMA1 demonstrated significantly greater stability compared with linear OMA1 mRNA (Fig. 1E). Additionally, circOMA1 exhibited resistance to RNase R digestion (which degrades linear RNA), while GAPDH and linear OMA1 mRNA were degraded, as confirmed by RNase R assay and agarose electrophoresis (Fig. 1F and G). Collectively, these results confirmed the successful generation of MMQ cell lines overexpressing circOMA1 and validated its circular nature and stability. To determine circOMA1 localisation, FISH and subcellular

fractionation were performed. Both methods revealed predominant cytoplasmic distribution of circOMA1 in circOM cells (Fig. 1H). Consistent with this, FISH analysis of PRL-PitNET-S and PRL-PitNET-R tissues showed circOMA1 localisation patterns similar to those observed in circOM cells (Fig. 1I).

circOMA1 promotes cell proliferation and resistance to CAB. To further confirm whether circOMA1 promoted CAB resistance, cell viability was assessed 72 h after treatment with increasing CAB concentrations (7.8125-250 μM). Dose-response analysis revealed that circOMA1 overexpression significantly increased CAB resistance, with the IC_{50} values of circOM (85.04±4.96 μM) exceeding that of circNC controls (51.17±3.81 μM) (Fig. 2A). For subsequent experiments, 50 μM CAB was used. Furthermore, the selected drug concentration was similar to or consistent with those used in previous studies (35-37). Notably, circOMA1 knockdown reversed CAB resistance in circOM cells (Fig. 2B and C). Furthermore, CCK-8, EdU incorporation and colony formation assays demonstrated that circOMA1 overexpression enhanced proliferation and colony formation in cells treated with CAB compared with the circNC cells (Fig. 2D-F and S1A). Given the pathognomonic hyperprolactinemia in PRL-PitNET, the effect of circOMA1 on PRL secretion was examined. circOMA1 overexpression elevated both PRL mRNA and protein levels (Fig. S1B-D). This phenotype correlated with increased expression of pituitary-specific positive transcription factor 1 (Pit-1), the master transcriptional regulator of PRL in PRL-PitNET (38). Consistently, it was further found that circOMA1 facilitated the expression of Pit-1 (Fig. S1E).

circOMA1 induces CAB resistance by attenuating autophagy and AKT dephosphorylation. Previous studies have demonstrated that CAB binds to DRD2 with high affinity, primarily exerting its effects through autophagy and inhibiting the AKT pathway (39). In the present study, it was revealed that circOMA1 markedly promoted AKT pathway activation and reduced the LC3-II/LC3-I ratio in circOM cells following CAB treatment (Fig. 2G). Consistent with this, TEM revealed a decrease in the number of autophagosomes in circOM cells compared with circNC cells after CAB exposure (Fig. 2H). To further investigate autophagic flux, western blotting showed decreased LC3-II/LC3-I and increased P62 (a late autophagy substrate) levels in circOM cells. This effect was amplified by co-treatment with the autophagy inhibitor 3-MA (Fig. 2I). Using the RFP-GFP-LC3 reporter assay (yellow puncta represent autophagosomes and red puncta represent autolysosomes due to GFP quenching in acidic lysosomes), results indicated fewer yellow puncta in circOM cells (Fig. 2J). Therefore, circOMA1 induced CAB resistance by attenuating autophagy and inhibiting the AKT pathway.

circOMA1 promotes the ubiquitination of DRD2, thereby inducing CAB resistance by upregulating KBTBD7. Previous studies have established that reduced expression or activity of DRD2 is a major cause of drug resistance in PRL-PitNET (8-11). Thus, whether circOMA1 promoted CAB resistance by regulating DRD2 was next assessed. The results showed that DRD2 protein levels were decreased in circOM (Fig. 3A), but its mRNA levels were not (Fig. S1F). Previous research identified that KBTBD7 [a substrate adaptor for the CUL3-RING ubiquitin (Ub) ligase complex] can specifically bind GABARAP proteins, ubiquitylate TIAM1 (40), and promote the ubiquitination of DRD2 (36). In the present study, accelerated degradation of DRD2 in circOM cells was observed following treatment with the protein synthesis inhibitor CHX (Fig. 3B), while accelerated degradation was reversed by co-treatment with the proteasome inhibitor MG132 (Fig. 3C). Furthermore, Co-IP assays revealed significantly increased ubiquitination of DRD2 protein in circOM cells (Fig. 3D). Similarly, KBTBD7 protein levels were markedly elevated in circOM (Fig. 3E). Subsequent immunofluorescence analysis of MMQ cells demonstrated cytoplasmic co-localisation of KBTBD7 and DRD2 (Fig. 3F), and Co-IP confirmed their physical interaction (Fig. 3G). Knocking down circOMA1 in circOM cells downregulated KBTBD7 and PRL expression while concomitantly upregulating DRD2 levels (Fig. 3H). To further elucidate whether circOMA1 regulated DRD2-mediated resistance specifically through KBTBD7, KBTBD7 expression was knocked out using CRISPR/Cas9 in circOM cells. This resulted in a significant increase in DRD2 expression (Fig. 3I and S2A-C), and a reversal of CAB resistance (Fig. 3J). Collectively, these findings indicated that circOMA1 induced CAB resistance by enhancing KBTBD7 expression, which in turn promoted DRD2 ubiquitination and degradation. Finally, in prolactinoma tissues, KBTBD7 expression was markedly higher in CAB-resistant (PRL-PitNET-R) cases than in controls, whereas DRD2 expression showed the opposite trend (Fig. 3K). Immunofluorescence also confirmed their co-localisation in the cytoplasm of these tumour tissues (Fig. 3L).

circOMA1 induces CAB resistance by regulating DRD2 through the miR-145-5p/KBTBD7 axis. The authors' previous research demonstrated that circOMA1 functioned as a sponge for miR-145-5p (33), and miR-145-5p expression was significantly reduced in PRL-PitNET-R (41). Consistently, miR-145-5p levels were lower in circOM (Fig. 4A), whereas circOMA1 knockdown increased miR-145-5p expression (Fig. 4B). This finding aligns with the low miR-145-5p expression observed in PRL-PitNET-R clinical samples (Fig. 4C). Therefore, it was hypothesised that miR-145-5p may regulate KBTBD7 expression by targeting its 3' untranslated region (UTR). Bioinformatics analysis using TargetScan (https://www.targetscan.org/vert_72/), miRWalk (http://mirwalk.umm.uni-heidelberg.de/) and miRDB (https://mirdb.org/index.html) identified potential binding sites for miR-145-5p within the KBTBD7 3'UTR (Fig. 4D). To validate this interaction, dual-luciferase reporter plasmids containing either the wild-type (WT) or mutated (Mut) KBTBD7 3'UTR sequence were established (Fig. 4E and F; Fig. S3). Co-transfection with miR-145-5p significantly reduced luciferase activity for the WT reporter but not the Mut reporter (Fig. 4G), confirming that miR-145-5p specifically targeted the KBTBD7 3'UTR.

To further investigate whether circOMA1 induced CAB resistance via the miR-145-5p/KBTBD7 axis regulating

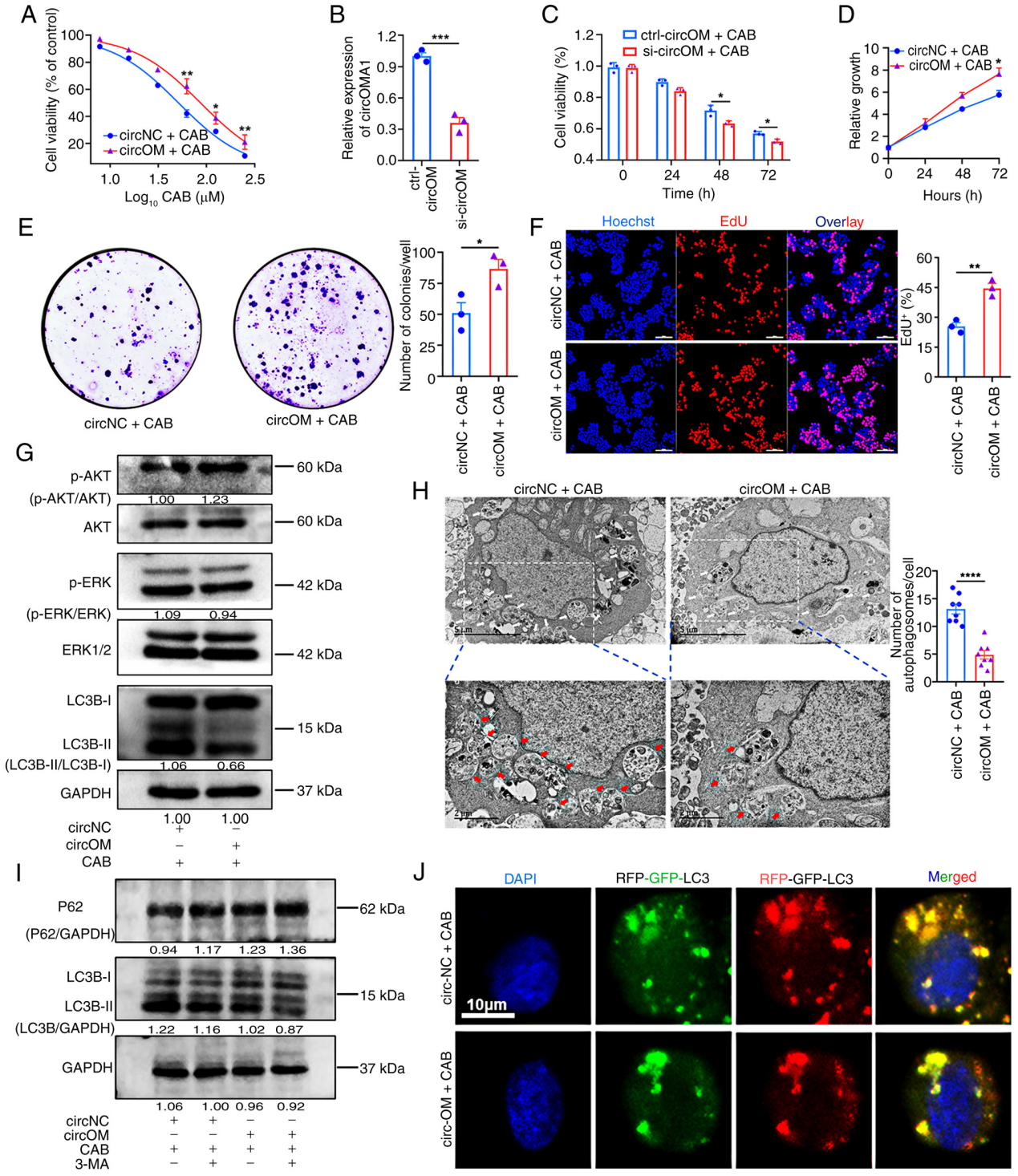

Figure 2. circOMA1promotes CAB resistance in PRL-PitNET cells through regulation of the autophagy pathway. (A) CCK-8 determination of IC_{50} in circOM and circNC cells after 72 h of treatment with a gradient of CAB concentrations (R^2=0.8611, 0.7030, 0.9248). (B) circOMA1 expression after 48 h of siRNA targeting. (C) Sensitivity of circOM cells to 50 μM CAB following circOMA1 knockdown (R^2=0.7891, 0.8357). (D-F) Representative images and quantification (right panels) of CCK-8, colony formation, and EdU assays used to assess the effect of circNC vs. circOM on CAB sensitivity. Scale bar, 100 μm. (G) Western blot analysis of LC3B, p-ERK1/2 and p-AKT in circNC and circOM cells after 72 h of treatment with 50 μM CAB. (H) Representative transmission electron microscopy images and quantification of autophagosomes in circNC (n=8) and circOM (n=8) cells after 72 h of treatment with 50 μM CAB. Scale bars, 5 and 2 μm; arrows indicate autophagosomes. (I) Western blot analysis of LC3B and p62 in circNC and circOM cells. (J) Representative confocal images of autophagic flux in circNC and circOM cells. Scale bar, 10 μm. Data are presented as the mean ± SEM of at least three repeats. Differences between groups were compared using an unpaired Student's t-test. *P<0.05, **P<0.01, ***P<0.001 and ****P<0.0001. CAB, cabergoline; NC, negative control; circ, circular RNA; PRL-PitNET, prolactin-secreting pituitary neuroendocrine tumour; siRNA, small interfering RNA; CCK-8, Cell Counting Kit-8; LC3B, microtubule-associated protein 1 light chain 3β; p-, phosphorylated.

DRD2, miR-145-5p levels were modulated in circOM cells. Overexpression of miR-145-5p significantly downregulated KBTBD7, upregulated DRD2, and enhanced CAB sensitivity in circOM cells. Conversely, knockdown of miR-145-5p

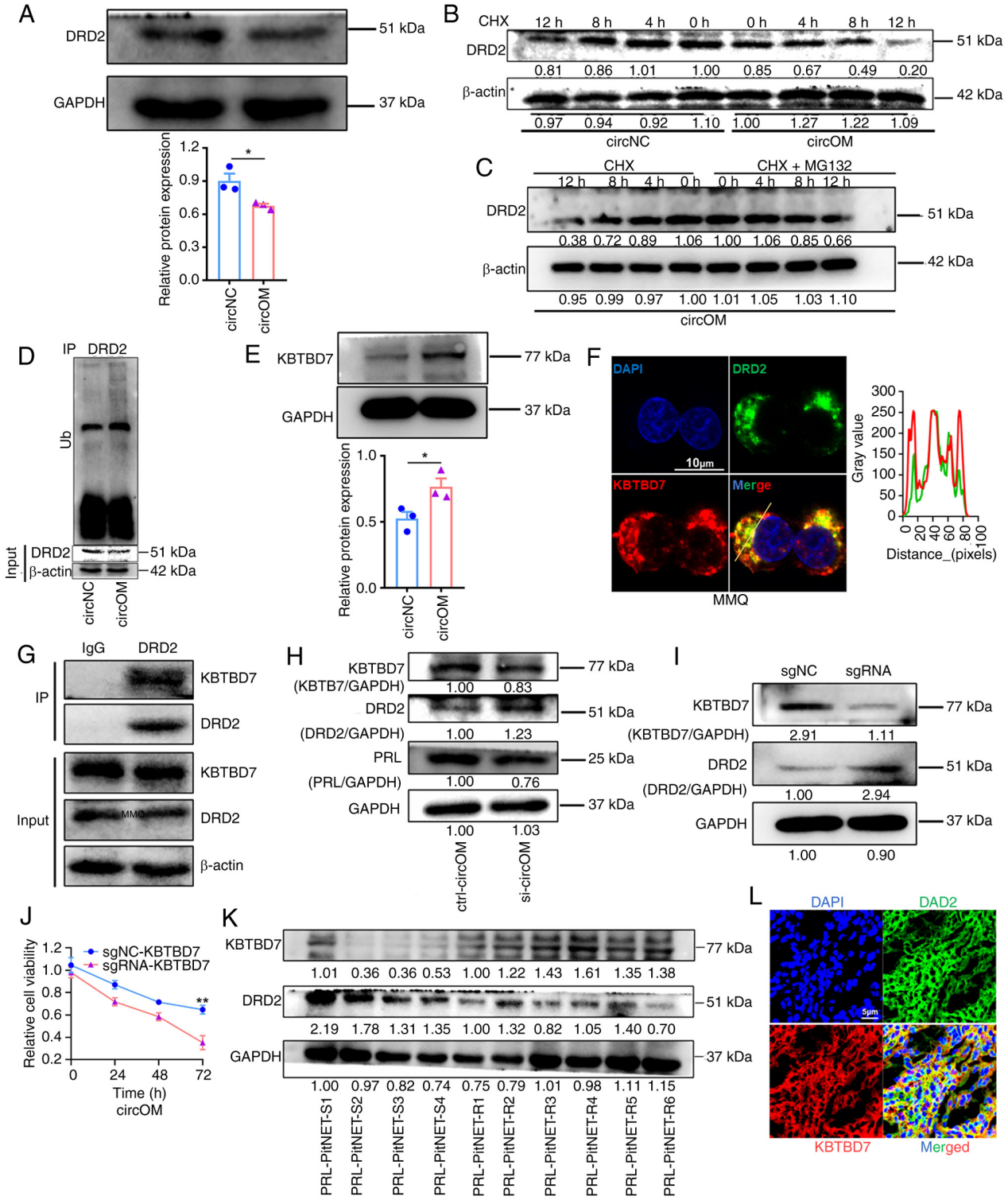

Figure 3. circOMA1 promotes ubiquitin-mediated degradation of DRD2 and induces CAB resistance in MMQ cells by upregulating KBTBD7. (A) Western blot detection of DRD2 protein in circNC and circOM cells (top) with quantification (bottom). (B) DRD2 protein levels in circNC and circOM cells were measured by western blotting after treatment with 100 μg/ml CHX for varying lengths of time. (C) Western blot analysis of DRD2 in circOM cells at the indicated time points after CHX treatment with or without treatment with 20 μM MG132. (D) Co-IP analysis of DRD2 ubiquitination in circNC and circOM cells (green arrow indicates DRD2). (E) Western blot and densitometric analysis of KBTBD7 expression in circNC and circOM cells. (F) Representative immunofluorescence images showing distribution and co-localisation of DRD2 and KBTBD7 in MMQ cells; the line profile at right indicates co-localisation. Scale bar, 10 μm. (G) Co-IP demonstrating the interaction between DRD2 and KBTBD7 in MMQ cells. (H) Immunoblot analysis of KBTBD7, DRD2 and PRL after circOMA1 knockdown for 72 h in circOM cells. (I) Immunoblot detection of DRD2 in circOM cells after KBTBD7 knockout by CRISPR/Cas9. (J) CCK-8 determination of circOM cell sensitivity to CAB after KBTBD7 knockdown (R^2=0.9240). (K) Western blot detection of KBTBD7 and DRD2 in PRL-PitNET-S (n=4) and PRL-PitNET-R (n=6) tissues. (L) Representative immunofluorescence images showing distribution and co-localisation of KBTBD7 and DRD2 in PRL-PitNET tissues. Scale bar, 10 μm. Data are presented as the mean ± SEM of at least three repeats. Differences between groups were compared using a unpaired Student's t-test. *P<0.05 and **P<0.01. CAB, cabergoline; NC, negative control; circ, circular RNA; PRL-PitNET, prolactin-secreting pituitary neuroendocrine tumour; PRL-PitNET-S, PRL-PitNET-sensitive; PRL-PitNET-R, PRL-PitNET-resistant; CHX, cycloheximide; MG132, proteasome inhibitor; CRISPR/Cas9, clustered regularly interspaced short palindromic repeats/CRISPR-associated protein 9; Co-IP, co-immunoprecipitation; circ, circular RNA; DRD2, dopamine D2 receptor; KBTBD7, Kelch-repeat and BTB domain-containing protein 7.

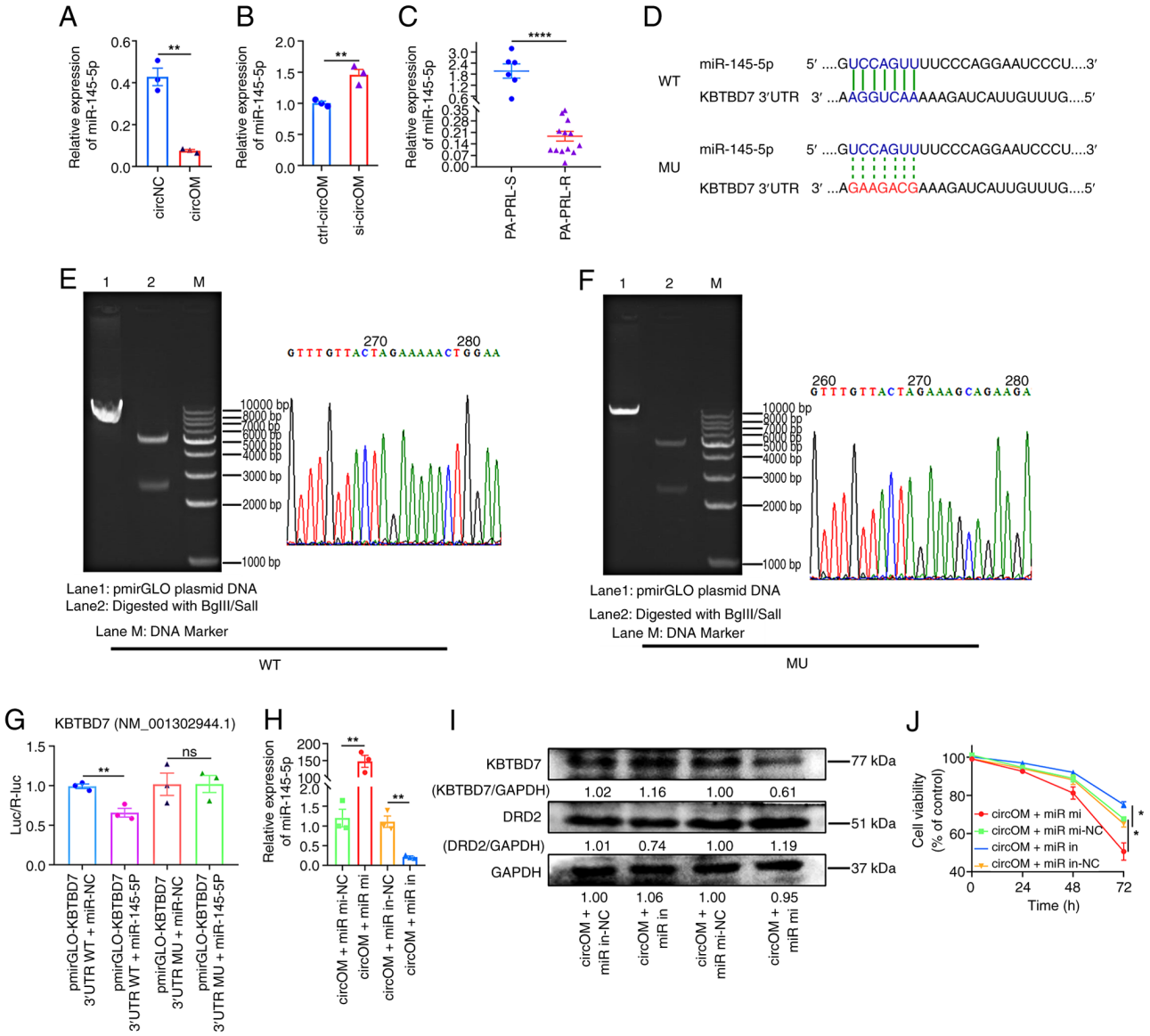

Figure 4. circOMA1 induces CAB resistance in MMQ cells by regulating DRD2 via a miR-145-5p/KBTBD7 axis. (A) RT-qPCR measurement of miR-145-5p levels in circNC and circOM cells. (B) miR-145-5p expression in circOM cells measured using RT-qPCR 48 h after circOMA1 knockdown. (C) RT-qPCR analysis of miR-145-5p in PRL-PitNET-S (n=6) and PRL-PitNET-R (n=13) tissues. (D-F) Bioinformatics prediction of miR-145-5p target sites in KBTBD7 and schematic of WT and MU dual-luciferase reporter constructs. (G) Dual-luciferase reporter assay confirming the miR-145-5p binding site in the KBTBD7 3'-UTR. (H) RT-qPCR of miR-145-5p in circOM cells 48 h after transfection with miR-145-5p mimic (miR-mi), mimic negative control (miR-mi-NC), miR-145-5p inhibitor (miR-in), or inhibitor negative control (miR-in-NC). (I) Western blot analysis of KBTBD7 and DRD2 protein levels in circOM cells 72 h after treatment with miR-145-5p mimic or inhibitor. (J) Cell Counting Kit-8 assay assessing circOM cell sensitivity to 50 μM CAB following treatment with miR-145-5p mimic or inhibitor (R^2=0.8246, 0.8094). Data are presented as the mean ± SEM of at least three repeats. Differences between groups were compared using an unpaired Student's t-test. *P<0.05, **P<0.01 and ****P<0.0001. ns, not significant; CAB, cabergoline; NC, negative control; circ, circular RNA; PRL-PitNET, prolactin-secreting pituitary neuroendocrine tumour; PRL-PitNET-S, PRL-PitNET-sensitive; PRL-PitNET-R, PRL-PitNET-resistant; RT-qPCR, reverse transcription-quantitative PCR; miR, microRNA; WT, wild-type; MU, mutant; UTR, untranslated region; KBTBD7, Kelch-repeat and BTB domain-containing protein 7.

produced the opposite effects (Fig. 4H-J). These results demonstrated that circOMA1 promoted CAB resistance by acting as a miR-145-5p sponge, thereby alleviating miR-145-5p-mediated repression of KBTBD7. Elevated KBTBD7 subsequently enhanced DRD2 ubiquitination and degradation, ultimately leading to drug resistance.

circOMA1 promotes proliferation and CAB resistance via exosomes. It has been previously demonstrated that exon-derived circRNAs are primarily located in the cytoplasm and are readily encapsulated into exosomes for secretion (42). Consistent with this, circOMA1, derived from the reverse splicing of an exon, was found to be predominantly distributed in the cytoplasm of MMQ cells using RNA-FISH and subcellular fractionation (Fig. 1H). To investigate whether circOMA1 was secreted via exosomes and whether it influenced parental tumour cell proliferation, a bilateral tumour model was established. MMQ cells were injected into the right flank of 4-6-week-old BALB/c nude mice, while circNC or circOM cells were injected into the contralateral flank (Fig. 5A). circOMA1 expressing tumours not only grew significantly faster but also promoted the growth of the contralateral

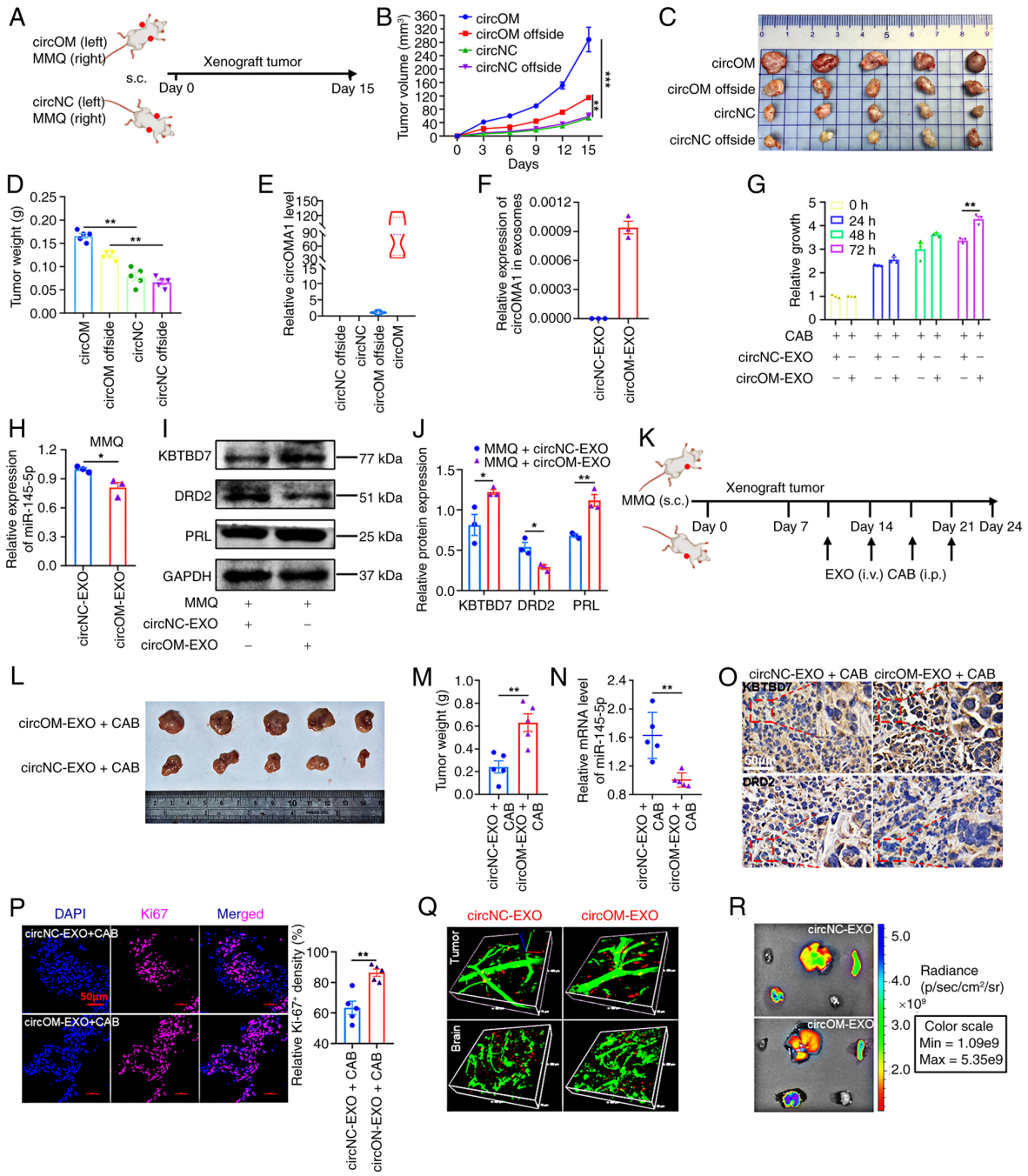

Figure 5. circOMA1 promotes parental cell proliferation and CAB resistance through exosomes. (A) *In vivo* pattern diagram of exosomes promoting parental cell proliferation. (B) Growth curve of subcutaneous tumours in nude mice. (C) Excised tumour images (n=5). (D) Mean tumour weight (n=5). (E) circOMA1 expression in subcutaneous tumours of nude mice detected using RT-qPCR (n=5). (F) RT-qPCR detection of circOMA1 expression in the exosomes from the supernatant of circNC or circOM cells. (G) Cell Counting Kit-8 assay of MMQ cell sensitivity to CAB when co-cultured with circNC-EXO or circOM-EXO (30 μg/ml of exosomes). (H) RT-qPCR detection of miR-145-5p in MMQ cells after 24 h co-culture with circNC-EXO or circOM-EXO. (I and J) Western blot detection and densitometric analysis of KBTBD7, DRD2 and PRL expression in MMQ cells after 72 h co-culture with circNC-EXO or circOM-EXO. (K) *In vivo* experimental diagram of exosome circOMA1-mediated CAB resistance. (L) Excised tumour images (n=5). (M) Mean tumour weight (n=5). (N) miR-145-5p expression in subcutaneous tumours of nude mice (n=5). (O) Representative immunohistochemistry images of KBTBD7 and DRD2 in subcutaneous tumours of nude mice. Scale bar, 50 μm. (P) Representative immunofluorescence image and quantification of Ki-67 expression in the subcutaneous tumours of nude mice. Scale bar, 50 μm. (Q) Representative microscopic distribution of exosomes in subcutaneous tumours, and in the brain of nude mice by live imaging assay 24 h after injection with 100 μg exosomes; green indicates blood vessels; red indicates exosomes. (R) Representative macroscopic distribution of exosomes in the heart, liver, spleen, lungs and kidneys of nude mice by live imaging assay 24 h after injection with 100 μg exosomes. Data are presented as the mean ± SEM of at least three repeats. Differences between groups were compared using an unpaired Student's t-test. *P<0.05, **P<0.01 and ***P<0.001. CAB, cabergoline; RT-qPCR, reverse transcription-quantitative PCR; EXO, exosomes purified from supernatant; KBTBD7, Kelch-repeat and BTB domain-containing protein 7; DRD2, dopamine receptor D2; PRL, prolactin.

parental MMQ tumours and exhibited higher final weights (Fig. 5B-D). Furthermore, circOMA1 was detected in the contralateral parental tumours opposite the circOM implants, but not in the circNC-injected mice (Fig. 5E). These findings suggest that circOMA1 may regulate tumour progression *in vivo* via exosomal transfer.

Subsequently, a Transwell co-culture system was used. MMQ cells were plated in the bottom chamber, while circOMA1 or circNC expressing cells were seeded in the upper chamber and co-cultured for 5 days (Fig. S4A). MMQ cells co-cultured with circOM cells exhibited significantly increased resistance to CAB (Fig. S4B). Supporting the exosomal involvement, the levels of circOMA1 in the conditioned medium decreased upon treatment with the exosome inhibitor GW4869 (Fig. S4C).

Next, exosomes were isolated and purified from the supernatant of circOM or circNC cells by differential ultracentrifugation (Fig. S4D). Using a nanoflow particle size analyser, the number and size of exosomes were determined. NTA confirmed the presence of exosomes, which predominantly ranged in diameter from 50-100 nm. Notably, the average diameter of exosomes from circOM supernatant (circOM-EXO) was larger than that from circNC supernatant (circOM-EXO) (Fig. S4E). Characterisation by flow cytometry using established exosomal markers (43), showed that both circOM-EXO and circNC-EXO expressed CD9 and CD63 (Fig. S4F), as well as ALG-2-interacting protein X (ALIX), tumour susceptibility gene 101 protein (TSG101) and HSP70 (Fig. S4G). TEM revealed the typical cup-shaped morphology and lipid bilayer structure of the isolated vesicles, with sizes consistent with NTA measurements (Fig. S4H). Critically, RT-qPCR showed circOMA1 expression specifically in circOM-EXO, but not in circNC-EXO (Fig. 5F). Interestingly, NTA also indicated that circOM cells secreted significantly more exosomes than circNC cells (Fig. S4I).

Given the established role of Rab family GTPases in exosome biogenesis and release (44-46), their expression was examined; only Rab27b was significantly upregulated in circOM cells compared with circNC cells (Fig. S4J). To assess exosome uptake by recipient cells, MMQ cells were incubated with PKH67-labelled circOM-EXO or circNC-EXO for 24 h. Laser confocal microscopy revealed that the labelled exosomes were internalised by MMQ cells and primarily localised to the cytoplasm (Fig. S5A). Flow cytometry further confirmed the uptake of both circOM-EXO and circNC-EXO by MMQ cells (Fig. S5B).

Finally, to determine if exosomal circOMA1 confers CAB resistance, purified circOM-EXO or circNC-EXO were directly co-cultured with MMQ cells. circOM-EXO significantly reduced the sensitivity of parental MMQ cells to CAB (Fig. 5G). Consistent with this functional transfer of resistance, EdU incorporation and colony formation assays yielded similar results (Fig. S6A and B).

Exosomal circOMA1 attenuates autophagy and AKT dephosphorylation to transmit resistance via the miR-145-5p/KBTBD7/DRD2 axis. Next, it was investigated whether exosomal circOMA1 also transmitted CAB resistance to recipient MMQ cells by regulating DRD2 through the miR-145-5p/KBTBD7 axis. First, co-culture of MMQ cells with circOM-EXO for 24 h significantly downregulated miR-145-5p levels in the recipient cells (Fig. 5H). Immunoblotting further revealed that after 72 h of co-culture, circOM-EXO significantly upregulated KBTBD7 and PRL protein expression while downregulating DRD2 protein levels in MMQ cells (Fig. 5I and J). Consistent with the protein data but contrasting with DRD2 mRNA (Fig. S6C), circOM-EXO upregulated Pit-1 mRNA levels (Fig. S6D). Moreover, following 72 h of co-culture, circOM-EXO significantly attenuated the CAB-induced dephosphorylation of AKT and autophagic response in MMQ cells (Fig. S6E-G).

To validate the *in vivo* relevance of this exosome-mediated resistance transmission via the miR-145-5p/KBTBD7/DRD2 axis, a xenograft tumour model was used. MMQ cells were subcutaneously inoculated into the right flanks of 4-6-week-old female BALB/c nude mice. Starting at day 10, mice received intravenous injections of circOM-EXO or circNC-EXO via the tail vein twice weekly for 2 weeks, combined with CAB treatment. Mice were euthanised on day 24 (Fig. 5K). The results demonstrated that circOM-EXO significantly enhanced tumour resistance to CAB, resulting in larger tumours and higher tumour weights in the circOM-EXO group compared with controls (Fig. 5L and M). Supporting the proposed axis, miR-145-5p levels were significantly decreased (Fig. 5N), and IHC revealed markedly elevated KBTBD7 protein expression alongside reduced DRD2 protein in circOM-EXO-treated tumours (Fig. 5O). Further corroborating the pro-tumorigenic role, circOM-EXO treatment considerably enhanced tumour cell proliferation, as evidenced by higher Ki-67 expression (Fig. 5P), and elevated levels of Pit-1 and PRL (Fig. S6H and I).

Finally, to track the biodistribution of administered exosomes *in vivo*, DID-labelled circNC-EXO or circOM-EXO were injected intravenously. Macro- and microscopic *in vivo* imaging performed 24 h post-injection revealed exosome enrichment in subcutaneous tumours, pituitary tissue and brain tissue, with lower abundance in the brain than in pituitary or tumours (Fig. S7A-C). For enhanced spatial resolution of exosome localisation within tissues, blood vessels were visualised using FITC-Dextran 2000. Microscopic imaging clearly showed internalised exosomes within subcutaneous tumours and brain tissue (Fig. 5Q). Macroscopic imaging of major organs confirmed strong exosomal fluorescence signals in the liver, spleen and lungs, but minimal signals in the heart and kidneys (Fig. 5R).

Exosomal circOMA1 can serve as a potential prognostic target. A series of previous studies have established that exosomal circRNAs can serve as potential biomarkers for tumour prognosis (23,24) and progression (28,29). To investigate the potential of exosomal circOMA1 as a prognostic biomarker in PitNETs, plasma exosomes isolated from elbow venous blood of patients with PitNET stratified by Knosp grade were assessed both pre- and post-operatively. TEM confirmed the presence of exosomes exhibiting the characteristic lipid bilayer membrane and cup-shaped morphology. Crucially, RT-qPCR analysis revealed a significant decrease in plasma exosomal circOMA1 levels following surgery (Fig. 6A-D). Analysis of clinical data also indicated that NF-PitNET had significantly higher Knosp grades than PRL-PitNET, GH-PitNET and ACTH-PitNET subtypes (Fig. 6E).

To further assess the broader prognostic potential of exosomal circOMA1, its relative expression abundance was assessed using the exoRBase V2 database (47) (http://www.exorbase.org/exoRBaseV2/help/toIndex) across healthy individuals, patients with various tumour types, and individuals with benign conditions. Database analysis demonstrated that

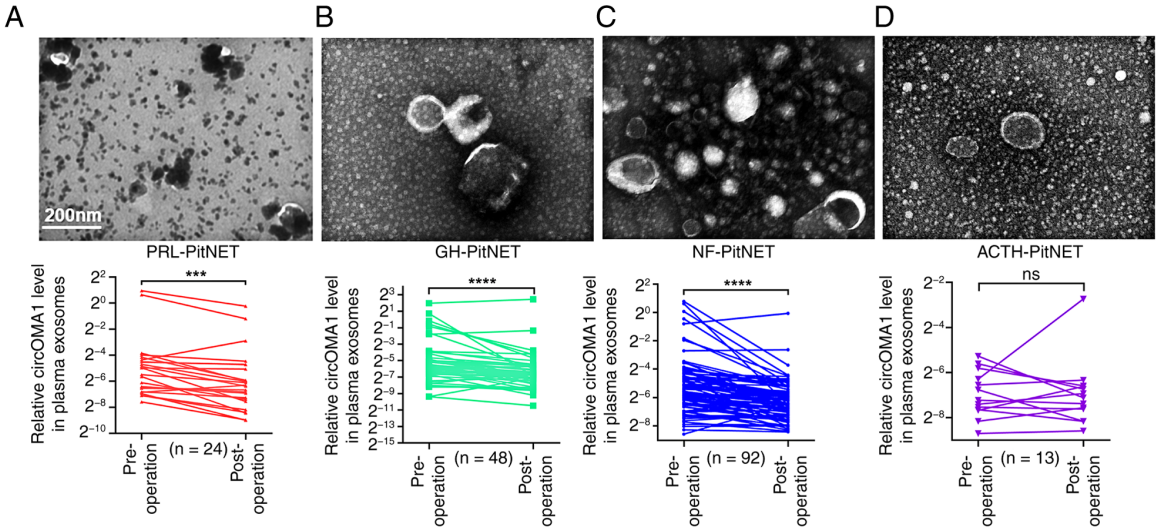

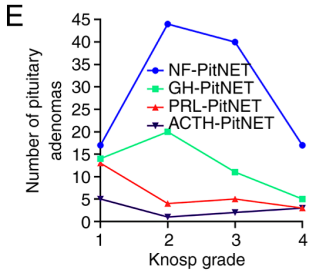

F

circID	circBase ID	Genomic position	chromosome	start	end	Strand	Gene symbol	Gene type	Detection frequency	Sample type	Tumor mean	Benign mean	Health mean
exo_circ_35788	hsa_circ_0002316	chr1:58506060-58539310	chr1	58506060	58539310	-	OMA1	protein coding gene	0.6	Blood	339.83	361.54	293.46

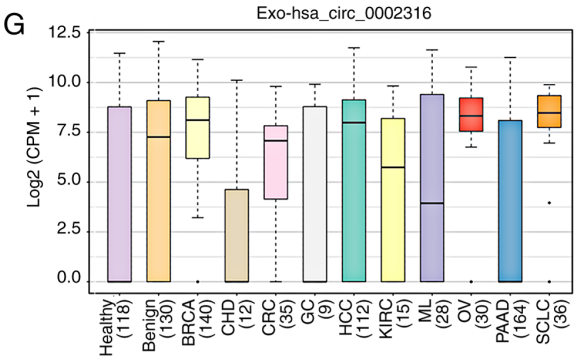

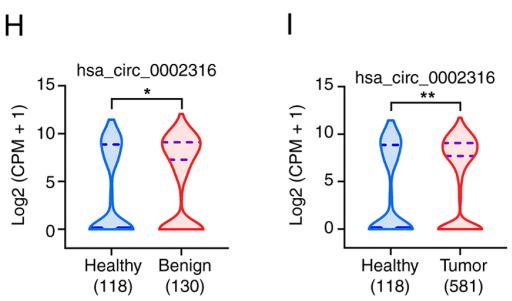

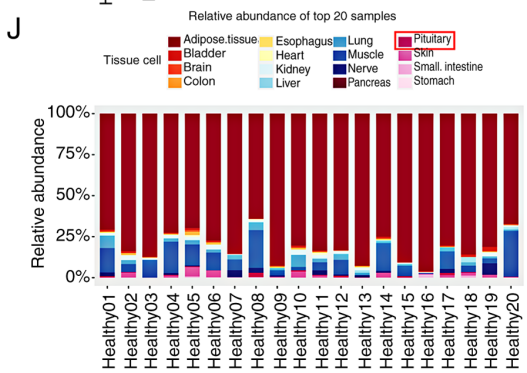

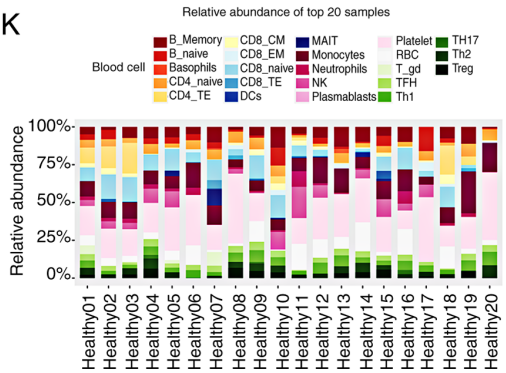

Figure 6. Exosomal circOMA1 can serve as a potential target for the management and prognosis of PitNETs. (A) Representative TEM images of plasma exosomes in patients with PRL-PitNET (top) and preoperative vs. postoperative expression levels of plasma exosomal circOMA1 (bottom) (n=24). (B) Representative TEM images of plasma exosomes in patients with GH-PitNET (top) and preoperative vs. postoperative expression levels of plasma exosomal circOMA1 (bottom) (n=48). (C) Representative TEM images of plasma exosomes in patients with NF-PitNET (top) and preoperative vs. postoperative expression levels of plasma exosomal circOMA1 (bottom) (n=92). (D) Representative TEM images of plasma exosomes in patients with ACTH-PitNET (top) and preoperative vs. postoperative expression levels of plasma exosomal circOMA1 (bottom) (n=13). (E) Knosp grade and corresponding number of PitNETs collected. (F) Expression information of blood exosomal circOMA1 across populations in the exosome database (http://www.exorbase.org/). (G) Specific expression of blood exosomal circOMA1 in different population types. (H) Difference in expression of blood exosomal circOMA1 between healthy and benign populations. (I) Difference in expression of blood exosomal circOMA1 between healthy and tumour populations. (J) Relative expression of circOMA1 in tissue cells of 20 healthy populations. (K) Relative expression of circOMA1 in blood cells of 20 healthy populations. Data are presented as the mean ± SEM of at least three repeats. Differences between groups were compared using a paired Student's t-test (A-D) or unpaired Student's t-test. *P<0.05, **P<0.01, ***P<0.001 and ****P<0.0001. Scale bar, 200 nm. circRNA, circular RNA; PitNET, pituitary neuroendocrine tumour; PRL-PitNET, prolactin-secreting PitNET; GH-PitNET, growth hormone-secreting PitNET; NF-PitNET, nonfunctioning PitNET; ACTH-PitNET, adrenocorticotropic hormone-secreting PitNET; RT-qPCR, reverse transcription-quantitative PCR; ns, not significant; TEM, transmission electron microscopy.

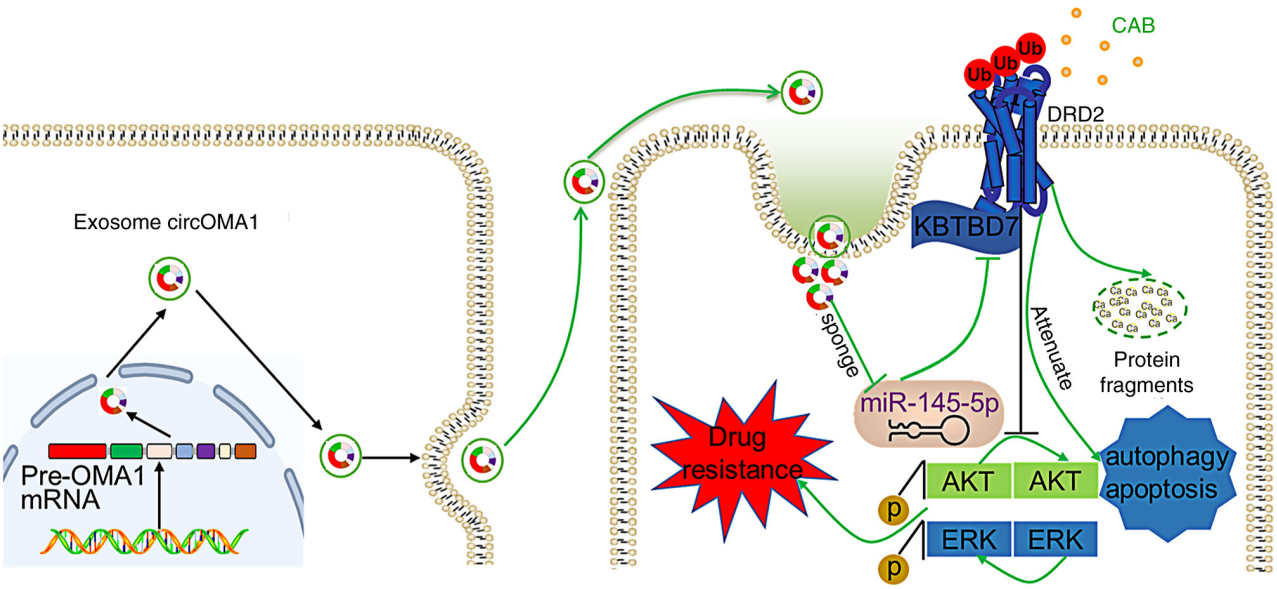

Figure 7. Schematic diagram of circOMA1 regulating the ubiquitination of DRD2 via a miR-145-5p/KBTBD7 axis to induce resistance in PRL-PitNET and transmit resistance through exosomes. circRNA, circular RNA; DRD2, dopamine receptor D2; miR, microRNA; KBTBD7, Kelch-repeat and BTB domain-containing protein 7; PRL-PitNET, prolactin-secreting pituitary neuroendocrine tumour.

the average expression level of exosomal circOMA1 in blood was markedly elevated in both tumour-bearing populations and those with benign conditions compared with healthy controls (Fig. 6F). Furthermore, specific tumour types (with less variation observed among the three categories) and benign conditions consistently showed considerably higher blood exosomal circOMA1 levels than healthy populations (Fig. 6G). Subsequent detailed analysis corroborated this elevation in tumour and benign populations relative to healthy individuals (Fig. 6H and I). Analysis of circOMA1 expression in tissue cells from 20 healthy individuals revealed relatively high abundance in the pituitary gland (Fig. 6J). Additionally, profiling circOMA1 expression and distribution in blood cells from these healthy donors indicated predominant enrichment in platelets (Fig. 6K).

Discussion

PRL-PitNET is the most common PitNET subtype and is the only subtype for which pharmacological therapy (such as CAB) is recommended as a first-line treatment. DAs normalise serum PRL levels, restore gonadal axis function, and reduce tumour dimensions in 80-90% of patients (48). Although most PRL-PitNET patients benefit from DA therapy, a subset exhibits resistance to DAs. Current clinical practice increasingly favours (CAB, a second-generation DA) for PRL-PitNET treatment due to its superior efficacy and reduced side-effect profile. Furthermore, the extended half-life of CAB (63-109 h) allows for convenient twice-weekly dosing (49). Int the present study, a previously unrecognised role for circOMA1 in mediating and propagating CAB resistance in PRL-PitNET was shown. These findings suggest a novel potential combination therapy strategy for overcoming CAB resistance in patients with a PRL-PitNET.

The biological functions of circRNAs include acting as transcriptional regulators, miRNA sponges, modulators of RNA stability, and interacting with RNA-binding proteins (50). A previous study by the authors found that circOMA1 bound to DRD2 with a complex formation score <0.5, suggesting a lack of stable binding capacity (33). In the present study, it was demonstrated that circOMA1 indirectly regulated DRD2 expression by sponging miR-145-5p, thereby influencing cellular sensitivity to CAB. It was previously established that CAB activated DRD2 to induce autophagy in MMQ cells, a process involving inhibition of the AKT pathway (39). In the present study, it was shown that circOMA1 attenuated autophagy and AKT pathway inhibition, consequently inducing CAB resistance in MMQ cells. Similarly, CAB also eliminated MMQ cells via the weak induction of apoptosis and activation of the ERK pathway (39). Consistent with this, it was observed that circOMA1-induced CAB resistance in MMQ cells involved attenuated autophagy, accompanied by slight inhibition of the ERK pathway. Although the majority of circRNAs function as non-coding RNAs, a previous study revealed that certain circRNAs can be translated into functional small peptides (33). Current research indicates circRNA translation occurs under two primary conditions: CircRNA contains both an open reading frame (ORF) and an internal ribosome entry site (IRES); and the 5' UTR of the circRNA possesses an m6A modification that facilitates translation (50). Sequence analysis revealed that circOMA1 contained one ORF and two IRES elements, indicating its potential for translation into functional peptides or proteins (51,52). Although preliminary predictions indicate that circOMA1 contains an ORF and an IRES, subsequent steps require the construction of separated fluorescent tags and tag antibodies targeting both flanking regions of the back-splicing junction of circOMA1. First, immunofluorescence and western blotting will be used to observe whether circOMA1 encodes a small peptide after circularisation. Second, the tagged small peptide will be identified by mass spectrometry using tag antibody labelling, followed by *in vitro* synthesis and functional

phenotypic validation in both cellular and animal models. Therefore, further investigation is warranted to determine whether circOMA1 contributes to PRL-PitNET resistance and progression via its translated products.

Immunoblotting and nanoflow cytometry analyses of exosomal marker proteins revealed differential protein expression profiles, consistent with prior research (53). *In vivo* experiments using microscopic and macroscopic live-imaging techniques clearly demonstrated significant enrichment of exosomes in tumours and the pituitary gland, indicating their ability to readily cross the blood-brain barrier. Conversely, exosome abundance in the brain parenchyma was markedly lower, likely due to the restrictive nature of the blood-brain barrier.

Exosomes represent an emerging, clinically promising detection modality, often referred to as a 'liquid biopsy.' This approach offers operational convenience and reduced patient discomfort compared with traditional tissue biopsy. In the present study, plasma exosomal circOMA1 levels generally decreased significantly following surgery in patients with a PitNET. Conversely, recurrent patients exhibited markedly elevated levels prior to a second surgery. This pattern likely reflects the reduction or absence of tumour-derived exosomal circOMA1 post-resection, with the decline being more pronounced in patients with longer postoperative intervals. Statistical analysis was not possible for certain patients due to the lack of pre- or post-operative blood samples. Furthermore, elevated blood exosomal circOMA1 expression was commonly observed across a range of other tumour types, while exhibiting relatively high abundance in the pituitary glands of healthy individuals. The relatively high expression of circOMA1 in pituitary tissues, along with its abnormally elevated expression in PRL-PitNETs, suggests that, in rat prolactinoma models, delivering circOMA1 knockdown molecules via exosomes may reduce circOMA1 expression in prolactinoma tissues to a lower level, potentially allowing for improved tumour control. Moreover, exoRBase database analysis reveals that circOMA1 is highly abundant in human platelets in peripheral blood, suggesting that platelet-derived exosomes may represent a feasible approach for identifying prognostic markers.

The present study adopted a translational research approach, starting from clinical observations in patients with prolactinoma, performing rigorous cellular and animal experiments to elucidate the underlying mechanism, and ultimately using clinical samples for validation. It was found that exosomal circOMA1 mediated drug resistance via the miR-145-5p/KBTBD7/DRD2 axis; however, several limitations remain: (i) Further validation using primary prolactinoma cells is required to confirm the functional relevance of the circOMA1/miR-145-5p/KBTBD7/DRD2 axis; (ii) in cellular and animal experiments, while exosome-delivered circOMA1 was shown to induce drug resistance, the potential contribution of other exosomal cargo cannot be excluded; (iii) while the sequences of circOMA1 and miR-145-5p in the rat MMQ cell line matched those in humans, and the rat and human DRD2 proteins share 95.71% similarity, potential species differences may still affect circRNA-miRNA interactions, DRD2 regulation and exosome biology; (iv) although the CAB concentration used in the *in vitro* experiments were consistent with prior reports, its extrapolation from cellular and animal models to clinical research requires further optimisation and validation; and (v) the cohort used to evaluate plasma exosomal circOMA1 as a prognostic biomarker was relatively small. In addition, although evidence that circOMA1 drives resistance in prolactinomas through exogenous overexpression/knockdown of circOMA1 was obtained, there is a lack of further validation on circOMA1 mutations. Despite the limitations, the present study nonetheless establishes that exosome-transferred circOMA1 is involved in prolactinoma drug resistance. Moving forward, multi-centre sample collection and optimisation of primary cell culture protocols may help overcome current challenges related to limited surgical samples and slow cell proliferation. Although postoperative patients showed significantly reduced plasma exosomal circOMA1 levels, further studies with larger sample sizes and advanced approaches, such as artificial intelligence-assisted analysis (based on the levels of plasma exosomal circOMA1, along with clinical and pathological diagnoses, machine learning was employed to establish baseline thresholds for artificial intelligence-assisted diagnosis), are warranted to strengthen these findings.

In conclusion, the results of the present study demonstrated that exosomal circOMA1 is crucial in the development and propagation of CAB resistance in PRL-PitNET. It was shown that circOMA1 regulates DRD2 via the miR-145-5p/KBTBD2 axis, thereby impairing downstream autophagy and inhibiting AKT pathway suppression, ultimately leading to CAB resistance. Furthermore, circOMA1 is transported by exosomes, facilitating the transmission of CAB resistance among MMQ cells both *in vitro* and *in vivo* (Fig. 7). Analysis of a large cohort of PitNETs samples suggested the potential of exosomal circOMA1 as a prognostic biomarker.

Acknowledgements

The authors would like to thank Dt Zhaoni Wang (The Third Affiliated Hospital of Sun Yat-sen University), for assisting in the experimental process, and Dr Qingping Lan (Zhongshan School of Medicine, Sun Yat-sen University) for providing plasmids.

Funding

The present study was supported by National Natural Science Foundation of China (grant nos. 82203179 and 82470816), and the Guangdong Provincial Natural Science Foundation (grant no. 2022A1515011265).

Availability of data and materials

The data generated in the present study may be requested from the corresponding author.

Authors' contributions

QR, DMZ, ZMW, SLZ, WLC and YHZ conceived the study. QR and YHZ designed the study. QR, XLL, WYH and NW collected the data. QR wrote the manuscript. QR, SKT and YHZ analysed and interpretated the data. All authors read and approved the final version of the manuscript. QR and YHZ confirm the authenticity of all the raw data.

Ethics approval and consent to participate

The present study was approved [approval no. (2020)090] by the Ethical Committee of the First Affiliated Hospital of Sun Yat-sen University (Guangzhou, China). Written informed consent was obtained from all patients.

Patient consent for publication

Not applicable.

Competing interests

The authors declare that they have no competing interests.

References

1. Tritos NA and Miller KK: Diagnosis and management of pituitary adenomas: A review. JAMA 329: 1386-1398, 2023.
2. Trouillas J, Jaffrain-Rea ML, Vasiljevic A, Raverot G, Roncaroli F and Villa C: How to classify the pituitary neuroendocrine tumors (PitNET)s in 2020. Cancers (Basel) 12: 514, 2020.
3. Villa C, Baussart B, Assié G, Raverot G and Roncaroli F: The World Health Organization classifications of pituitary neuroendocrine tumours: A clinico-pathological appraisal. Endocr Relat Cancer 30: e230021, 2023.
4. Auriemma RS, Pirchio R, De Alcubierre D, Pivonello R and Colao A: Dopamine agonists: From the 1970s to today. Neuroendocrinology 109: 34-41, 2019.
5. Bevan JS, Webster J, Burke CW and Scanlon MF: Dopamine agonists and pituitary tumor shrinkage. Endocr Rev 13: 220-240, 1992.
6. Molitch ME: Pharmacologic resistance in prolactinoma patients. Pituitary 8: 43-52, 2005.
7. Maiter D: Management of dopamine agonist-resistant prolactinoma. Neuroendocrinology 109: 42-50, 2019.
8. Wu ZB, Zheng WM, Su ZP, Chen Y, Wu JS, Wang CD, Lin C, Zeng YJ and Zhuge QC: Expression of D2RmRNA isoforms and ERmRNA isoforms in prolactinomas: Correlation with the response to bromocriptine and with tumor biological behavior. J Neurooncol 99: 25-32, 2010.
9. Shimazu S, Shimatsu A, Yamada S, Inoshita N, Nagamura Y, Usui T and Tsukada T: Resistance to dopamine agonists in prolactinoma is correlated with reduction of dopamine D2 receptor long isoform mRNA levels. Eur J Endocrinol 166: 383-390, 2012.
10. Bueno C, Trarbach EB, Bronstein MD and Glezer A: Cabergoline and prolactinomas: Lack of association between DRD2 polymorphisms and response to treatment. Pituitary 20: 295-300, 2017.
11. Pivonello C, Patalano R, Negri M, Pirchio R, Colao A, Pivonello R and Auriemma RS: Resistance to dopamine agonists in pituitary tumors: Molecular mechanisms. Front Endocrinol (Lausanne) 12: 791633, 2021.
12. Song ZJ, Reitman ZJ, Ma ZY, Chen JH, Zhang QL, Shou XF, Huang CX, Wang YF, Li SQ, Mao Y, *et al*: The genome-wide mutational landscape of pituitary adenomas. Cell Res 26: 1255-1259, 2016.
13. Jiang X and Zhang X: The molecular pathogenesis of pituitary adenomas: An update. Endocrinol Metab (Seoul) 28: 245-254, 2013.
14. Dance A: Circular logic: Understanding RNA's strangest form yet. Nature 635: 511-513, 2024.
15. Hu K, Liu X, Li Y, Li Q, Xu Y, Zeng W, Zhong G and Yu C: Exosomes Mediated Transfer of Circ_UBE2D2 Enhances the Resistance of Breast Cancer to Tamoxifen by Binding to MiR-200a-3p. Med Sci Monit 26: e922253, 2020.
16. Pan Z, Zheng J, Zhang J, Lin J, Lai J, Lyu Z, Feng H, Wang J, Wu D and Li Y: A novel protein encoded by exosomal circATG4B Induces oxaliplatin resistance in colorectal cancer by promoting autophagy. Adv Sci (Weinh) 9: e2204513, 2022.
17. Wang X, Chen T, Li C, Li W, Zhou X, Li Y, Luo D, Zhang N, Chen B, Wang L, *et al*: CircRNA-CREIT inhibits stress granule assembly and overcomes doxorubicin resistance in TNBC by destabilizing PKR. J Hematol Oncol 15: 122, 2022.
18. Li L, Li W, Chen N, Zhao H, Xu G, Zhao Y, Pan X, Zhang X, Zhou L, Yu D, *et al*: FLI1 exonic circular RNAs as a novel oncogenic driver to promote tumor metastasis in small cell lung cancer. Clin Cancer Res 25: 1302-1317, 2019.
19. Pan B, Qin J, Liu X, He B, Wang X, Pan Y, Sun H, Xu T, Xu M, Chen X, *et al*: Identification of serum exosomal hsa-circ-0004771 as a novel diagnostic biomarker of colorectal cancer. Front Genet 10: 1096, 2019.
20. Wen N, Peng D, Xiong X, Liu G, Nie G, Wang Y, Xu J, Wang S, Yang S, Tian Y, *et al*: Cholangiocarcinoma combined with biliary obstruction: An exosomal circRNA signature for diagnosis and early recurrence monitoring. Signal Transduct Target Ther 9: 107, 2024.
21. Liu Y, Li Y, Zang J, Zhang T, Li Y, Tan Z, Ma D, Zhang T, Wang S, Zhang Y, *et al*: CircOGDH is a penumbra biomarker and therapeutic target in acute ischemic stroke. Circ Res 130: 907-924, 2022.
22. Zhang X, Xu Y, Ma L, Yu K, Niu Y, Xu X, Shi Y, Guo S, Xue X, Wang Y, *et al*: Essential roles of exosome and circRNA_101093 on ferroptosis desensitization in lung adenocarcinoma. Cancer Commun (Lond) 42: 287-313, 2022.
23. He YD, Tao W, He T, Wang BY, Tang XM, Zhang LM, Wu ZQ, Deng WM, Zhang LX, Shao CK, *et al*: A urine extracellular vesicle circRNA classifier for detection of high-grade prostate cancer in patients with prostate-specific antigen 2-10 ng/mL at initial biopsy. Mol Cancer 20: 96, 2021.
24. Wang J, Zhang Q, Zhou S, Xu H, Wang D, Feng J, Zhao J and Zhong S: Circular RNA expression in exosomes derived from breast cancer cells and patients. Epigenomics 11: 411-421, 2019.
25. Théry C, Ostrowski M and Segura E: Membrane vesicles as conveyors of immune responses. Nat Rev Immunol 9: 581-593, 2009.
26. Liu Y, Ma L, Hua F, Min Z, Zhan Y, Zhang W and Yao J: Exosomal circCARM1 from spheroids reprograms cell metabolism by regulating PFKFB2 in breast cancer. Oncogene 41: 2012-2025, 2022.
27. Zheng R, Zhang K, Tan S, Gao F, Zhang Y, Xu W, Wang H, Gu D, Zhu L, Li S, *et al*: Exosomal circLPAR1 functions in colorectal cancer diagnosis and tumorigenesis through suppressing BRD4 via METTL3-eIF3h interaction. Mol Cancer 21: 49, 2022.
28. Ding L, Zheng Q, Lin Y, Wang R, Wang H, Luo W, Lu Z, Xie H, Ren L, Lu H, *et al*: Exosome-derived circTFDP2 promotes prostate cancer progression by preventing PARP1 from caspase-3-dependent cleavage. Clin Transl Med 13: e1156, 2023.
29. Yao X, Mao Y, Wu D, Zhu Y, Lu J, Huang Y, Guo Y, Wang Z, Zhu S, Li X and Lu Y: Exosomal circ_0030167 derived from BM-MSCs inhibits the invasion, migration, proliferation and stemness of pancreatic cancer cells by sponging miR-338-5p and targeting the Wif1/Wnt8/β-catenin axis. Cancer Lett 512: 38-50, 2021.
30. Xiong Y, Tang Y, Fan F, Zeng Y, Li C, Zhou G, Hu Z, Zhang L and Liu Z: Exosomal hsa-miR-21-5p derived from growth hormone-secreting pituitary adenoma promotes abnormal bone formation in acromegaly. Transl Res 215: 1-16, 2020.
31. Zhang Y, Liu YT, Tang H, Xie WQ, Yao H, Gu WT, Zheng YZ, Shang HB, Wang Y, Wei YX, *et al*: Exosome-Transmitted lncRNA H19 inhibits the growth of pituitary adenoma. J Clin Endocrinol Metab 104: 6345-6356, 2019.
32. Mao ZG, He DS, Zhou J, Yao B, Xiao WW, Chen CH, Zhu YH and Wang HJ: Differential expression of microRNAs in GH-secreting pituitary adenomas. Diagn Pathol 5: 79, 2010.
33. Du Q, Hu B, Feng Y, Wang Z, Wang X, Zhu D, Zhu Y, Jiang X and Wang H: circOMA1-Mediated miR-145-5p suppresses tumor growth of nonfunctioning pituitary adenomas by targeting TPT1. J Clin Endocrinol Metab 104: 2419-2434, 2019.
34. Livak KJ and Schmittgen TD: Analysis of relative gene expression data using real-time quantitative PCR and the 2(-Delta Delta C(T)) Method. Methods 25: 402-408, 2001.
35. Jian F, Sun Y, Sun Q, Zhang B and Bian L: NEK2 regulates cellular proliferation and cabergoline sensitivity in pituitary adenomas. J Cancer 12: 2083-2091, 2021.
36. Liu YT, Liu F, Cao L, Xue L, Gu WT, Zheng YZ, Tang H, Wang Y, Yao H, Zhang Y, *et al*: The KBTBD6/7-DRD2 axis regulates pituitary adenoma sensitivity to dopamine agonist treatment. Acta Neuropathol 140: 377-396, 2020.

37. Wu N, Zhu D, Li J, Li X, Zhu Z, Rao Q, Hu B, Wang H and Zhu Y: CircOMA1 modulates cabergoline resistance by downregulating ferroptosis in prolactinoma. J Endocrinol Invest 46: 1573-1587, 2023.
38. Scully KM, Jacobson EM, Jepsen K, Lunyak V, Viadiu H, Carrière C, Rose DW, Hooshmand F, Aggarwal AK and Rosenfeld MG: Allosteric effects of Pit-1 DNA sites on long-term repression in cell type specification. Science 290: 1127-1131, 2000.
39. Tang C, Sun R, Wen G, Zhong C, Yang J, Zhu J, Cong Z, Luo X and Ma C: Bromocriptine and cabergoline induce cell death in prolactinoma cells via the ERK/EGR1 and AKT/mTOR pathway respectively. Cell Death Dis 10: 335, 2019.
40. Genau HM, Huber J, Baschieri F, Akutsu M, Dötsch V, Farhan H, Rogov V and Behrends C: CUL3-KBTBD6/KBTBD7 ubiquitin ligase cooperates with GABARAP proteins to spatially restrict TIAM1-RAC1 signaling. Mol Cell 57: 995-1010, 2015.
41. Jian M, Du Q, Zhu D, Mao Z, Wang X, Feng Y, Xiao Z, Wang H and Zhu Y: Tumor suppressor miR-145-5p sensitizes prolactinoma to bromocriptine by downregulating TPT1. J Endocrinol Invest 42: 639-652, 2019.
42. Lyu D and Huang S: The emerging role and clinical implication of human exonic circular RNA. RNA Biol 14: 1000-1006, 2017.
43. Lötvall J, Hill AF, Hochberg F, Buzás EI, Di Vizio D, Gardiner C, Gho YS, Kurochkin IV, Mathivanan S, Quesenberry P, *et al*: Minimal experimental requirements for definition of extracellular vesicles and their functions: A position statement from the International Society for Extracellular Vesicles. J Extracell Vesicles 3: 26913, 2014.
44. Savina A, Vidal M and Colombo MI: The exosome pathway in K562 cells is regulated by Rab11. J Cell Sci 115 (Pt 12): 2505-2515, 2002.
45. Hsu C, Morohashi Y, Yoshimura S, Manrique-Hoyos N, Jung S, Lauterbach MA, Bakhti M, Grønborg M, Möbius W, Rhee J, *et al*: Regulation of exosome secretion by Rab35 and its GTPase-activating proteins TBC1D10A-C. J Cell Biol 189: 223-232, 2010.
46. Ostrowski M, Carmo NB, Krumeich S, Fanget I, Raposo G, Savina A, Moita CF, Schauer K, Hume AN, Freitas RP, *et al*: Rab27a and Rab27b control different steps of the exosome secretion pathway. Nat Cell Biol 12: 19-30; sup pp 1-13, 2010.
47. Qi Y, Xu R, Song C, Hao M, Gao Y, Xin M, Liu Q, Chen H, Wu X, Sun R, *et al*: A comprehensive database of exosome molecular biomarkers and disease-gene associations. Sci Data 11: 210, 2024.
48. Glezer A and Bronstein MD: Prolactinomas. Endocrinol Metab Clin North Am 44: 71-78, 2015.
49. Curran MP and Perry CM: Cabergoline: A review of its use in the treatment of Parkinson's disease. Drugs 64: 2125-2141, 2004.
50. Pisignano G, Michael DC, Visal TH, Pirlog R, Ladomery M and Calin GA: Going circular: History, present, and future of circRNAs in cancer. Oncogene 42: 2783-2800, 2023.
51. Song R, Guo P, Ren X, Zhou L, Li P, Rahman NA, Wołczyński S, Li X, Zhang Y, Liu M, *et al*: A novel polypeptide CAPG-171aa encoded by circCAPG plays a critical role in triple-negative breast cancer. Mol Cancer 22: 104, 2023.
52. Huang D, Zhu X, Ye S, Zhang J, Liao J, Zhang N, Zeng X, Wang J, Yang B, Zhang Y, *et al*: Tumour circular RNAs elicit anti-tumour immunity by encoding cryptic peptides. Nature 625: 593-602, 2024.
53. Yim KHW, Krzyzaniak O, Al Hrout A, Peacock B and Chahwan R: Assessing extracellular vesicles in human biofluids using flow-based analyzers. Adv Healthc Mater 12: e2301706, 2023.